

1 **Light-evoked activity and BDNF regulate mitochondrial dynamics and**  
2 **mitochondrial localized translation.**

3  
4 Alex Kreymerman<sup>1,2\*</sup>, Jessica E. Weinstein<sup>2\*</sup>, Sahil H. Shah<sup>1,3</sup>, David N. Buickians<sup>1</sup>, Anne Faust<sup>4</sup>,  
5 Yolandi Van Der Merwe<sup>4</sup>, Michael M. Nahmou<sup>1</sup>, In-Jae Cho<sup>1</sup>, Star K. Huynh<sup>1</sup>, Sonya Verma<sup>1</sup>,  
6 Xiao-Lu Xin<sup>2</sup>, Michael B. Steketee<sup>2,4</sup>, Jeffrey L. Goldberg<sup>1</sup>

7  
8 1. Byers Eye Institute, Stanford University, Palo Alto, CA 94303

9 2. University of Miami Miller School of Medicine, Miami, FL 33136

10 3. Medical Scientist Training Program, University of California, San Diego, CA 92093

11 4. Department of Ophthalmology and McGowan Institute for Regenerative Medicine, University  
12 of Pittsburgh, Pittsburgh, PA 15213

13  
14 \*These authors contributed equally.

15  
16 Address correspondence to:

17 Jeffrey L. Goldberg

18 Byers Eye Institute

19 Stanford University

20 2452 Watson Ct

21 Palo Alto, CA 94303

## 22 **Abstract**

23 Mitochondria coordinate diverse functions within neurites, including signaling events for axonal  
24 maintenance, and degeneration. However, less is known about the role of mitochondria in axon  
25 development and maturation. Here we find that in maturing retinal ganglion cells (RGCs) in vivo,  
26 axonal mitochondria increase in size, number, and total area throughout development. We  
27 demonstrate through multiple approaches in vivo that the mechanism underlying these  
28 mitochondrial changes are dependent on eye opening and associated neuronal activity, which can  
29 be mimicked by brain derived neurotrophic factor (BDNF). We report downstream gene and  
30 protein expression changes consistent with mitochondrial biogenesis and energetics pathways, and  
31 present evidence that the associated transcripts are localized and translated at mitochondria within  
32 axons in an activity-dependent manner. Together these data support a novel model for  
33 mitochondrial-localized translation in support of intra-axonal mitochondrial dynamics and axonal  
34 maturation.

35

## 36 **Introduction**

37 Neurons are among the highest metabolically active cell types in the body. This is due in part to  
38 mitochondrial oxidative phosphorylation highly coupled with the energy demand generated by  
39 electrophysiologic activity and associated signaling<sup>1-3</sup>. Beyond ATP production, mitochondrial  
40 activities such as calcium homeostasis, fatty acid oxidation, secondary messenger and signaling  
41 pathway modulation also participate in supporting neurons and their extensive axonal  
42 compartments<sup>4</sup>. Mitochondrial activities are critically dependent on the expression and assembly  
43 of approximately 600-1500 proteins encoded in the nucleus<sup>5-12</sup>, yet mitochondria can be separated  
44 down the axon by a meter or more from the cell body<sup>13</sup>.

45

46 As a result, such cells have evolved unique mechanisms for maintaining continuous  
47 communication between mitochondria and the nucleus<sup>14</sup>. These include shuttling mitochondria  
48 and their nuclear-encoded proteins up and down axons using motor proteins kinesins and  
49 dyneins<sup>15-18</sup>. Transported mitochondria are also capable of undergoing fusion or fission with  
50 neighboring mitochondria, acquiring or shedding genetic material and proteins<sup>19</sup>. Finally, new  
51 mitochondria can also be assembled and packaged with nuclear and mitochondrial encoded  
52 proteins, in a process known as mitochondrial biogenesis. This process takes place in the  
53 perinuclear space and within axons, leading to increased numbers of mitochondria in neuronal  
54 compartments<sup>20-22</sup>. Together these changes in mitochondrial localization, size and total cellular  
55 volume are referred to as mitochondrial dynamics.

56

57 An additional mechanism implicated in supplying nuclear proteins to distal axonal mitochondria  
58 is the transport and then local translation of RNA in axonal compartments (reviewed elsewhere<sup>23</sup>).  
59 Interestingly, many investigations indicate that a consistent and major portion of axon-localized  
60 transcripts encode nuclear proteins that regulate mitochondrial functions<sup>24-27</sup>. Additionally,  
61 nuclear-encoded mitochondrial transcripts have been shown to physically localize on/in  
62 mitochondrial membranes<sup>28-32</sup>, with further evidence suggesting that mitochondria can act as local  
63 translation sites<sup>33-35</sup>. However, it is not yet known how such localization is regulated. Here we find  
64 that developmental changes in axonal mitochondria are regulated by activity in vivo, and explore  
65 associated regulation of mRNA expression and localization by activity in RGCs in vitro.

66

67 **Results**

68 Mitochondrial networks reorganize at the time of eye opening

69 We first studied mitochondrial organization in RGC axons in transgenic mice expressing cyan  
70 fluorescent protein (CFP) fused to the COX8a mitochondrial targeting sequence under control of  
71 the Thy-1 promoter (Thy1-CFP/COX8A). In this mouse, approximately 5% of RGCs express the  
72 CFP/COX8a transgene, permitting visualization and quantification of mitochondria in RGC axons  
73 (Figure 1A,B). We used this mouse model to investigate axon-specific mitochondrial networks at  
74 postnatal (P) days 9, 12, 15, and 45, as RGCs experience significant developmental changes  
75 through this time period<sup>28-31,36-39,40-44</sup>. Of note, these time points also follow the period of  
76 developmental cell death in RGCs, which peaks at P5 in mice<sup>45-47</sup>, thus allowing for the  
77 identification of mitochondrial changes independent of cell death signaling, which can influence  
78 mitochondrial morphology<sup>48,49</sup>. Analysis of CFP-labeled mitochondria in whole mount retinas and  
79 optic nerves by confocal microscopy revealed significant reorganization in RGC axons throughout  
80 postnatal development (Figure 1B). Overall, mitochondria increased in size, number, and occupied  
81 a greater percentage of axonal area from P9 to P45 (Figure 1C-E). Interestingly, within a relatively  
82 short window of development, around eye opening (P12/13 to P15), mitochondrial size, number,  
83 and occupied area increased in both RGC retinal and optic nerve axon segments, with optic nerve  
84 mitochondria experiencing the greatest change during this time window.

85  
86 Although Thy-1 gene expression peaks around P12 in RGCs and continues to be stably expressed  
87 throughout adulthood<sup>50</sup>, and thus Thy-1 promoter-related artifacts are unlikely, mitochondria size  
88 changes from P12-P15 were also confirmed by transmission electron microscopy (TEM; Figure  
89 2). Specifically, mitochondrial size, number, and occupied area increased in RGC axons from P12  
90 to P15 by 25%, 105%, and 31% respectively (Figure 2B, C, D). Thus by both fluorescence and

91 TEM imaging, RGC axon mitochondrial size, number, and occupied area increase during this  
92 developmental window.

93

#### 94 Eye opening regulates mitochondrial networks

95 As eye opening occurs between P12-P15 with a concomitant significant increase in visual activity,  
96 we asked whether the mitochondrial morphological changes are dependent on eye opening in CFP-  
97 COX8a mice with surgically premature or delayed eye opening. (Figure 3A). For premature eye  
98 opening, we surgically opened the P10 eyelid margin, two days prior to normal eye opening, and  
99 allowed animals to mature to P12. We found increases in mitochondrial size, number and occupied  
100 area in retinal and optic nerve axons compared to unopened P12 eyes (Figure 3B, C, D). Thus eye  
101 opening accelerates the mitochondrial morphology changes identified in normal development.

102

103 Conversely, to determine if eye opening is necessary for the developmental increases in  
104 mitochondrial size, number, and occupied area from P12-15, we delayed eye opening by suturing  
105 eyelids shut at P11, prior to natural eye opening, then allowed mice to mature to P15, delaying eye  
106 opening by 2-3 days (Figure 3A). Compared to age-matched controls, the delayed eye opening  
107 model led to significant decreases in all mitochondrial measurements (Figure 3B, C, D), in most  
108 cases back to levels found in P12 animals. Thus, these data suggest that the process of eye opening  
109 is sufficient and necessary for the mitochondrial network increases found from P12-15.

110

#### 111 RGC activity and BDNF regulate mitochondrial networks

112 These findings suggested the hypothesis that light-stimulated electrical activity in axons (i.e.,  
113 action potentials) contribute to the observed changes in axon mitochondrial distribution and

114 morphology. To test the contribution of electrical activity to axonal mitochondrial changes during  
115 the period of eye opening, we pharmacologically inhibited both spontaneous and light-evoked  
116 electrical activity in RGCs by intravitreally injecting tetrodotoxin (TTX)<sup>51</sup> prior to eye opening at  
117 P11 and again after eye opening at P13, followed by mitochondrial quantification at P15. We found  
118 that TTX but not control vehicle injection inhibited mitochondrial increases in size in retinal and  
119 optic nerve axons (Figure 4A, B), and mitochondrial number and occupied area only in the optic  
120 nerve portion of RGC axons (Figure 4C, D), in all cases to levels equivalent to vehicle injected  
121 P12 animals. Thus RGC electrical activity is a significant contributor to mitochondrial network  
122 changes that occur concomitant with eye opening. However, discrepancies in mitochondrial  
123 numbers and area within retinal versus optic nerve axons likely indicate additional regulation that  
124 contributes to mitochondrial dynamics during this period.

125  
126 Downstream of electrical activity, BDNF expression has been shown to be regulated by eye  
127 opening and to be blocked by TTX injection<sup>36</sup>, and to modulate mitochondrial dynamics<sup>36,52-55</sup>. To  
128 determine whether BDNF could rescue the inhibitory effects of TTX on mitochondrial networks,  
129 BDNF and TTX were co-injected at P11 and again at P13, and mitochondrial parameters were  
130 measured at P15. BDNF was capable of significantly reversing the TTX-induced decreases in  
131 mitochondrial size, and showed a non-significant trend towards such rescue in mitochondrial  
132 number and occupied area in optic nerve axons (Figure 4B-D). Of note, this rescue effect of BDNF  
133 was only detected in the optic nerve but not retinal axons (Figure 4A), suggesting again that  
134 different mechanisms regulate mitochondrial dynamics in a compartment-specific manner within  
135 the axon. Furthermore, when BDNF was injected at P10 and mitochondrial parameters were  
136 measured at P12, BDNF did not increase mitochondrial size, number or area on its own (Figure

137 4A-D). Nonetheless, these data suggest that activity and BDNF are both critical in regulating the  
138 morphology and distribution of optic nerve axon mitochondria during this stage of visual system  
139 development.

140

#### 141 Activity and BDNF regulate the expression of nuclear encoded mitochondrial genes

142 To investigate molecular mechanisms associated with activity and BDNF, we explored the  
143 transcriptional influence of exogenously added BDNF and TTX on nuclear-encoded mitochondrial  
144 gene expression in RGCs. To accomplish this, we injected TTX and/or BDNF in combination or  
145 alone at P11 and P13, acutely purified RGCs from P15 retinas, and extracted RNA for qRT-PCR  
146 gene arrays. We then analyzed expression data and conducted pathway analysis. Major upstream  
147 regulators were identified by probing the gene expression sets for targets of known regulators, and  
148 then filtering for genes whose expression was concordant with the inhibitory effects of TTX and  
149 subsequent rescue with BDNF on mitochondrial morphology and distribution (Figure 5A). The  
150 resulting analysis revealed that PGC1- $\alpha$  and RICTOR, master mitochondrial dynamics and  
151 energetics modulators, were putative upstream regulators of genes modulated by TTX and/or  
152 BDNF (Figure 5B, C). For many mitochondria genes regulated by RICTOR and PGC1- $\alpha$ , TTX  
153 and BDNF showed opposing effects on expression. In most cases, the gene expression profile of  
154 TTX+BDNF mimicked that of BDNF alone, suggesting BDNF's effects on gene expression were  
155 dominant over effects of TTX and placing BDNF downstream of activity. Furthermore, BDNF  
156 increased basal and maximum respiratory capacity in purified RGCs in vitro even in the presence  
157 of TTX (Figure 5D), consistent with pathways predicted by these gene expression changes.  
158 Ontological analysis of these gene expression datasets suggested opposing functions between  
159 BDNF and TTX, with fission/fusion and mitochondrial biogenesis pathways induced by BDNF

160 and suppressed by TTX (Figure 5E, F), consistent with our *in vivo* data.

161

162 Activity regulates mitochondrial associated local translation and mitochondrial dynamics

163 Our gene arrays showed that expression of many of the mitochondrial genes assayed were  
164 suppressed by TTX-mediated inhibition of activity. To investigate whether transcription or  
165 translation activity were being globally downregulated in RGCs by activity inhibition, we treated  
166 RGCs with 5-ethynyluridine (EU), a uridine analog, or O-propargyl-puromycin (OPP), a  
167 puromycin analog. These molecules readily incorporate into newly synthesized RNAs (with EU)  
168 or proteins (with OPP), and can be conjugated to fluorophores with click chemistry to visualize  
169 the location and relative amount of synthesis taking place within cells<sup>56,57</sup>. Using this approach,  
170 we first tested whether TTX inhibited transcription or translation by intravitreally injecting TTX  
171 at P11 and P13, and then pulsing with EU or OPP at P15 for 1hr. Upon visualization, no detectable  
172 differences in signal intensity from EU or OPP were identified in retinas (Figure 6A), suggesting  
173 that transcription and translation were not broadly inhibited by activity suppression.

174

175 However, because of the potential variability with labeling efficiency, either from injection site  
176 differences, variations in injection volumes, and/or kinetics of intravitreal injection dispersion, we  
177 followed up *in vivo* experiments with *in vitro* approaches where EU and OPP labeling can be better  
178 controlled and quantified. For *in vitro* approaches, RGCs were isolated to 99% purity by  
179 immunopanning from early postnatal mouse retinas and seeded at low density, allowing for the  
180 visualization of individual cells and neurites. Then, cells were virally transduced to fluorescently  
181 label mitochondria with a Cox8a targeted dsRED, cultured for 48hrs, treated with TTX for 2hrs,  
182 and finally pulsed for 15 min or 1hr with OPP or EU, respectively. The cells were treated with



183 TTX for a shorter period of time than during in-vivo experiments to avoid significant changes in  
184 viability, which at early postnatal days has the potential to decrease cell survival, unlike the in vivo  
185 time points tested<sup>58</sup>. However, no detectable decrease in viability after 2hr of TTX incubation was  
186 detected (Figure 6B). In RGCs in vitro, we again found cells with intensely labeled peri-nuclear  
187 regions, but no discernable differences in new transcript or protein levels in the cell body regions  
188 (Figure 6C), similar to in vivo experiments. Interestingly, in OPP-treated cells, obvious puncta  
189 were also visible in axonal segments. These puncta appeared scattered throughout distal axon  
190 segments in axonal tips, with varying sizes and numbers (Figure 6D). To see if activity inhibition  
191 by TTX could influence the presence of these axon-localized OPP puncta, we quantified the  
192 abundance of OPP sites within axonal segments, and found that TTX-treated axons demonstrate  
193 significant decreases (~70%) in the number of OPP puncta as compared to controls, similar to the  
194 effects of translational inhibitor cycloheximide (Figure 6E), suggesting that activity regulates  
195 axon-localized protein synthesis. Note that these changes in puncta number are not likely due to  
196 decreased transport of newly synthesized proteins from the cell body, as the rate of soluble protein  
197 transport is less than 0.1  $\mu\text{m/s}$  (or 90  $\mu\text{m}$  in 15 min) and would be an unlikely captured change  
198 within the assay window in distal RGC axons<sup>59</sup>, which are typically longer than 600 $\mu\text{m}$  at 48hrs  
199 of culture in these cells<sup>60</sup>.

200  
201 Axon-localized protein translation has been previously described<sup>31</sup>, but to further examine axon  
202 localized OPP puncta we immunostained cells with an antibody against cytoplasmic ribosomal  
203 protein S3, an integral component of the 40s-ribosomal subunit translation initiation site<sup>61</sup>. In these  
204 cells, we found a significant level of co-localization of ribosomal protein S3 with OPP puncta and  
205 interestingly a large majority of these OPP puncta also colocalized with mitochondria (Figure

206 6F,G), suggesting that the detected axon-localized OPP puncta active local translation sites are  
207 often at or near mitochondria. Similar to our in vivo results, we further found that mitochondrial  
208 size decreased in TTX-treated RGCs (Figure 6H) and was increased in the presence of BDNF,  
209 which was dominant over the effect of TTX, with increases or decreases in mitochondrial size  
210 correlating with increases or decreases in OPP-to-mitochondria localization (.499 r) (Figure 6J).  
211 Of note, these puncta were not visible in EU-treated cells, which is either a reflection of the  
212 abundance of RNA within axons or an indication of detection limitations. Thus new protein  
213 synthesis is detected at mitochondria and together with mitochondrial network size shows a  
214 dependence on electrical activity in RGC axons.

215

#### 216 RNA binding proteins tether nuclear encoded mitochondrial mRNA to mitochondria

217 To investigate the potential for mitochondria to act as docking sites for nuclear-encoded  
218 mitochondrial mRNA and new protein translation and, we conducted proteomic and qRT-PCR  
219 experiments on mitochondria purified from optic nerves or retinas. Briefly, isolation of axonal  
220 mitochondria was performed by incubating homogenized whole optic nerve tissue with a  
221 magnetically conjugated Translocase Of Outer Mitochondrial Membrane 22 (TOM22) antibody.  
222 Then, homogenates were passed through magnetic columns to remove cytosolic contaminants,  
223 followed by extensive washing, elution, and the pelleting of mitochondria<sup>62</sup> (Figure 7A). We used  
224 a number of approaches to validate this relatively novel purification protocol. First, isolated  
225 mitochondria were examined by SEM and TEM, which showed that mitochondrial membranes  
226 and cristae architecture were structurally maintained after isolation with dark puncta visible on the  
227 outside of mitochondria (Figure 7B), representing nanoparticle-bound TOM22 and confirming the  
228 integrity of outer mitochondrial membranes after isolation. On western blots, isolated

229 mitochondria maintained proteins from all complexes in the electron transport chain (Figure 7C)  
230 and inner and outer membrane integrity proteins (Figure 7D) but no detectable cytoplasmic  
231 GAPDH (Figure 7E). Of note, supernatant fractions from TOM22-purified mitochondria, which  
232 would reflect TOM22-bound membranes from ruptured, non-intact mitochondria, had no  
233 detectable ETC or membrane integrity proteins (Figure 7C, D), suggesting that nearly all TOM22-  
234 purified mitochondria were intact and captured in the pellet fraction. Finally, TOM22-selected  
235 optic nerve mitochondria were isolated from Thy-1-CFP/COX8a mice and further purified to  
236 axon-specific mitochondria through a traditional fluorescence acquired cell sorting (FACS)  
237 machine. In all FACS assays, mitochondria from Thy-1-CFP/COX8a mice retained membrane  
238 integrity proteins, detected by western blot (Figure 7F), and CFP positivity, detected by  
239 mitotracker-CMXROS co-staining(Figure 7G). Furthermore, isolated CFP<sup>+</sup> mitochondria  
240 maintained high membrane potentials and readily took up JC-1, forming distinct populations of  
241 red shifted J-aggregate-retaining mitochondria (Figure 7H) that lost polarization in response to a  
242 membrane potential uncoupler, carbonyl cyanide-4-(trifluoromethoxy) phenylhydrazone (FCCP)  
243 (Figure 7I, J). Overall, these data suggest that isolating optic nerve axon mitochondria via magnetic  
244 columns and FACS yields relatively pure and structurally intact mitochondria, with surface and  
245 internal proteins and functional polarization maintained throughout the procedure.

246  
247 We next examined these purified mitochondria for association with nuclear-encoded RNA binding  
248 proteins and translation-associated proteins from 3 young mouse optic nerves and also whole  
249 retinas by mass spectrometry, which yielded a total of 427 identifiable proteins after pooling all 6  
250 samples. We cross-referenced these identified proteins with MitoCarta2.0, maintained by MIT's  
251 Broad Institute, a database of thoroughly vetted proteins that co-purify with mitochondria<sup>8,10</sup>.

252 Using this approach, we were able to stratify our proteins into three groups of proteins based on  
253 evidence of mitochondrial localization (Figure 8A, B), 210 canonical mitochondrial proteins based  
254 on MitoCarta data from proteomics, computation, and microscopy analysis, 154 non-canonical  
255 mitochondrial proteins in the MitoCarta database that correlate with less pure mitochondrial  
256 fractions, and 63 proteins that are likely non-mitochondrial and do not show up in the MitoCarta  
257 database. Of course some of these “non-mitochondrial” proteins may still be mitochondrial as the  
258 MitoCarta data was not compiled from the visual system, where there could be uniquely-localized  
259 mitochondrial proteins.

260  
261 After filtering for this external validation of mitochondrial association, we looked for the subset  
262 of proteins with predicted RNA binding potential by filtering proteins through David<sup>63</sup>, Panther<sup>64</sup>,  
263 and Uniport<sup>65</sup> data bases using the gene ontology term RNA binding. Proteins that met these  
264 criteria were then cross-referencing against datasets from the RNA-protein interactome of cardiac  
265 cells<sup>66</sup>, HEK cells<sup>67</sup>, and HeLa cells<sup>68</sup>, as well as RNA binding protein databases AtTRACT and  
266 RBPDB<sup>69-72</sup>. This yielded the identification of 71 proteins with RNA binding properties, of which  
267 43 had published evidence of direct interaction with mitochondria(Figure 8C, D). These included  
268 proteins with roles in translation, RNA processing, and RNA shuttling.

269  
270 Since these data suggested that nuclear-encoded RNA binding proteins associate with  
271 mitochondria, we then asked whether there was also evidence for an association of nuclear-  
272 encoded mRNA on purified mitochondria. We purified mitochondria as above, extracted total  
273 RNA from pellets, and assayed for the presence of mRNA by qRT-PCR arrays. This identified a  
274 range of nuclear-encoded mitochondrial mRNAs, including genes that regulate mitochondrial

275 dynamics, cell death, and energetics (Figure 9A,B). All detected mRNAs amplified in less than 30  
276 cycles, lending confidence to the integrity of these measurements.

277

278 To directly test the potential for mRNA tethering to outer mitochondrial membranes by RNA  
279 binding proteins, as implied by the OPP imaging experiments, mass spectrometry, and qRT-PCR  
280 array data, we treated mitochondrial isolates with Proteinase K to release surface proteins and  
281 associated mRNA, and then pelleted treated mitochondria to assay by qPCR for mRNAs released  
282 in the supernatant fractions (Figure 10A). As in Figure 8, to ensure that mRNAs detected in these  
283 assays were specific to mitochondria, we also verified the relative purity of mitochondrial fractions  
284 by western blotting for the presence of cytoplasmic contaminants, using actin an additional control  
285 (Figure 10B). We also took measures to verify that Proteinase K treatment did not release proteins  
286 from the interior of mitochondria, as shown by western blots against Complex III-Core Protein 2  
287 and Complex V alpha subunit proteins (Figure 10C). In addition, there was no significant decrease  
288 in mitochondrial encoded mRNA ND4 in mitochondrial pellets and no significant increase in  
289 supernatant fractions (Figure 10D), providing strong evidence that Proteinase K did not interfere  
290 with inner mitochondrial protein or RNA. However, when purified mitochondria were tested for  
291 the release of nuclear-encoded mRNAs by Proteinase K, we found a significant number of mRNAs  
292 were released from mitochondrial pellets into the corresponding supernatant fraction, as compared  
293 to controls (Figure 10D). These mRNAs coded for proteins known to regulate mitochondrial  
294 dynamics, biogenesis, energetics, and RNA transport. We also found mRNA encoding cytoplasmic  
295 proteins GAPDH and actin bound to mitochondria, suggesting that bound mRNAs are not limited  
296 to those coding for mitochondrial-specific proteins. Interestingly, when we pre-treated in vivo with  
297 TTX at P11 and P13 and then assayed purified retinal mitochondrial transcripts from P15 mice,

298 there were essentially no significant changes in mitochondrial localized mRNAs dependent on  
299 activity, although this could reflect an under sampling error as RGCs make up less than 1% of  
300 retinal cells. Overall, these data indicate that mitochondria bind nuclear-encoded mRNAs known  
301 to modulate mitochondrial size, number, and energetics, and that this process is mediated by RNA  
302 binding proteins present on mitochondrial membranes.

303

## 304 **Discussion**

305 Proper CNS neuron development and homeostasis depends critically on mitochondrial  
306 organization and function throughout distal axonal segments. Furthermore, mitochondria have to  
307 be capable of dynamically changing to meet intra-axonal demands distal to the cell body. As result,  
308 neurons and their distal segments have particularly demanding requirements for the active  
309 expression, trafficking, and assembly of nuclear-encoded-mitochondrial-macromolecules  
310 (proteins and mRNAs). Here we build upon the known mechanisms regulating rapid mitochondrial  
311 change in axons, and present new findings in which mitochondria size, number, and total area are  
312 regulated via activity and BDNF, and implicate a role for associated activity-regulated  
313 mitochondrial localized translation in regulating distal mitochondrial dynamics in CNS axons.

314

### 315 Activity and BDNF regulate mitochondrial morphology and localization

316 Concomitant with eye opening, the visual system experiences increases in RGC electrical activity  
317 and BDNF expression, triggered by  $Ca^{+2}$  signaling and the activation of CREB-mediated  
318 transcription<sup>52,73-75</sup>. Both activity and BDNF signaling play a pivotal role in axon development,  
319 including axon growth and presynaptic maturation, with mitochondrial dynamics and energetics  
320 having stereotyped roles in these developmental events (reviewed elsewhere<sup>76</sup>). Yet, the link

321 between activity or BDNF signaling and changes in mitochondrial dynamics during CNS axon  
322 maturation in vivo had not been investigated. Here we show that RGC activity and downstream  
323 BDNF during eye opening is sufficient and necessary to increase mitochondrial size and number  
324 in RGCs' optic nerve axons during development, and that activity also plays a similar, albeit more  
325 muted role, in regulating mitochondrial morphology in RGCs' retinal axon segments. Whether this  
326 dependence is also observed during earlier periods of RGC development, e.g. when RGCs  
327 experience correlated waves of activity generated by amacrine cells before eye opening, or in other  
328 developing neurons, will be important questions to pursue.

329  
330 In addition, we provide data supporting a new model in which activity and BDNF are modulating  
331 mitochondrial dynamics, biogenesis, and energetics in part through gene expression and local  
332 protein translation. Analysis of gene expression data pointed to the activation of transcriptional  
333 networks linked to PGC1- $\alpha$  and RICTOR by activity and BDNF during the period of eye opening,  
334 similar to findings in other neurons<sup>77</sup>. Furthermore, cellular energetics are linked to PGC1- $\alpha$ <sup>78</sup> and  
335 RICTOR<sup>79</sup> signaling, and our data reflected these findings<sup>80</sup>, and suggest that activity and BDNF  
336 also regulate basal respiration in RGCs, with BDNF increasing the maximum respiration capacity  
337 of RGCs regardless of activity inhibition. Thus, our data is indicative of a generalized increase in  
338 mitochondrial biogenesis activity in RGCs treated with BDNF (and vice versa with TTX  
339 treatment), a mechanism by which morphology and distribution along axons may be regulated.  
340 Overall, these data also support a pathway in which eye opening and subsequent increased  
341 neuronal firing signal to modulate the expression of mitochondrial related transcription,  
342 mitochondrial dynamics, and energetics. There may also be a direct protein-based signaling  
343 cascade triggered by activity and subsequent BDNF signaling onto mitochondria, since there is

344 evidence that activity and BDNF increase respiration independent of nuclei in mitochondria-  
345 containing synaptosomal preparations<sup>53,81,82</sup>.

346

347 Activity regulates a novel mechanism of mitochondrial localized translation

348 Axon segments can be up to a meter away from a neuron's cell body and nucleus, presenting a  
349 challenge for signaling and subsequent renewal of proteins required for normal neuronal function.

350 Axonal transport of nuclear-encoded proteins, in which nuclear proteins are translated in the  
351 perinuclear space and transported down axons at rates of up to 8 mm/day for soluble proteins (i.e.

352 metabolic enzymes) or 100 and even 400 mm/day when associated with mitochondria or  
353 neuropeptide containing vesicles, respectively<sup>59,83,84</sup>, may not be quick enough to resupply distal

354 axonal sites at times of rapid demand. In addition, nuclear-encoded mRNAs including some for  
355 mitochondrial proteins<sup>24-26</sup> are transported to distal axon sites including in RGC axons in the

356 mouse<sup>27</sup>, ready to be translated locally and on demand<sup>23</sup>, suggesting that mitochondria function is  
357 in part maintained by active axonal localized translation. Consistent with our findings, activity

358 modulation and neurotrophic factors including BDNF regulate local translation in xenopus  
359 neurons<sup>85,86</sup> and our extend this model showing that such translation occurs at mitochondria in an

360 activity-dependent manner. The enrichment in mRNAs encoding mitochondrial proteins on or near  
361 mitochondria<sup>28-32</sup> and the finding that ribosomes can directly bind to mitochondria membranes via

362 TOM proteins and act in co-translation protein import in yeast<sup>33-35</sup>, together suggest a novel  
363 mechanism whereby increased neuronal firing and BDNF downstream signaling pathways directly

364 regulate mitochondrial dynamics through modified local translation (Figure 12). This model will  
365 require additional molecular investigation in mammalian axons, such as the development of

366 approaches to inhibit protein synthesis in specific subcellular compartments.



367

368 Implications for aging and disease

369 These data move towards identifying mechanisms regulating mitochondrial organization and  
370 nuclear-encoded mitochondrial transcript localization in CNS axons during normal developmental,  
371 but raise questions to what degree similar mechanisms act in aging or neurodegenerative disease.  
372 Declining or defective mitochondrial function has been linked to many neurodegenerative  
373 diseases<sup>87</sup>. In humans and in mammalian animal models, defective axonal mRNA transport  
374 mechanisms have been implicated in the pathogenesis of neuropathies including spinal muscle  
375 atrophy, amyotrophic lateral sclerosis, and distal hereditary neuropathy<sup>88-90</sup>, and declining  
376 metabolic function is increasingly linked to reduced expression of mitochondrial transcripts<sup>91,92</sup>.  
377 Thus, understanding how the expression and local translation of nuclear mitochondrial transcripts  
378 are regulated and how these influence mitochondrial function may yield new approaches to treat  
379 dysfunction in the nervous system.

380

381 **Materials and Methods**

382 **Animal use statement.** Experiments conformed to the ARVO Statement for the Use of Animals  
383 in Ophthalmic and Vision Research and were approved by the Stanford University Biosafety  
384 Committee and the Institutional Animal Care and Use Committee. Strains used in these  
385 experiments included wild type CD-1, C57BL/6, and B6.Cg-Tg(Thy1-CFP/COX8A)S2Lich/J  
386 mice (The Jackson Laboratory).

387

388 **Cell Culture.** RGCs were purified from male and female postnatal day 1/2 (P1/2) C57BL/6 mice  
389 (Charles River Laboratories) by immunopanning, and cultured on poly-D-lysine- (10 µg/mL;

390 Sigma Aldrich, P-6407) and laminin-coated (2  $\mu\text{g}/\text{mL}$ ; Sigma, L-6274) cover glass bottom 96 well  
391 plates (Greiner Bio-One)<sup>93,94</sup>, in media with or without BDNF supplement as previously  
392 described<sup>86</sup>. Then, RGCs were treated with baculoviruses to label mitochondria (BacMam 2.0,  
393 Thermo Fisher Scientific, C10601) and 48 hrs later incubated with pharmacological agents, at  
394 stated concentrations and times. In RNA or protein labeling experiments RGCs were incubated  
395 with EU for 2 hrs or OPP for 15 min (according to the Click-iT Nascent RNA or Protein Synthesis  
396 Assay Kit from Thermo Fisher Scientific, C10327 or C10456). After all incubations cells were  
397 then fixated (4% PFA PBS), permeabilized (0.5% Triton PBS), and in EU- or OPP-incubated  
398 cells, Click labeling reaction were performed. To identify ribosomes, cells were incubated with  
399 antibodies against ribosomal protein S3 (Cell Signaling Technology, D50G7) at 1:100 overnight  
400 at 4°C, and secondary Alexa-647 conjugated antibodies at 1:500 for 2hrs at room temperature. To  
401 label growth cones, cells were incubated with Alexa Fluor® 647 Phalloidin (Thermo Fisher  
402 Scientific, A22287) at 1:40 room temp. for 30 min prior to confocal imaging. In oxygen  
403 consumption experiments, RGCs were plated as described above, with or without BDNF, at  
404 40k/well in 96 well plates designed for the Seahorse XF96 instrument (Agilent, 101085-004). After  
405 culturing for 24hrs, media was exchanged with Assay Media (Agilent, 102365-100) and FluxPak  
406 injectable ports were loaded with drugs as recommended by mitochondrial stress test kit (Agilent,  
407 103015-100). TTX was loaded in the empty port A as the first injection, followed by Oligomycin,  
408 FCCP, and Rotenone/Antimycin A, respectively. After assay was complete oxygen consumption  
409 values were normalized to the number of Dapi positive cells per well.

410

411 **Imaging.** B6.Cg-Tg(Thy1-CFP/COX8A)S2Lich/J mice (CFP/COX8a, Jackson labs) were  
412 euthanized and perfused with 4% PFA in PBS at P9, P13, P15, and P45. Perfused animals were

413 then enucleated and the eyes and the optic nerves post-fixed in 4% PFA for 1-3 hours. Post fixed  
414 tissues were whole mounted on slides in Vecta-Shield mounting medium (Vector Labs, #H-1400)  
415 and imaged on a Zeiss LSM 710 confocal microscope. Compressed Z-stacks were analyzed by  
416 selecting nine random 25 x 50  $\mu\text{m}$  sections and then measuring CFP expression with the ImageJ  
417 particle analyzer tool (National Institutes of Health). All images of cultured RGCs were collected  
418 on a Zeiss LSM 880 confocal system with a 40x/63x objective and using airyscan imaging mode,  
419 followed by airyscan processing using Zen software. Mitochondrial size, translation spot size, and  
420 colocalization analysis was conducted using Volocity Imaging Software (Perkin Elmer).

421  
422 **Electron microscopy.** Adult CD-1 mice under anesthesia were perfused with one half  
423 Karnovsky's fixative; 2.5% glutaraldehyde and 2% paraformaldehyde (PFA) in 0.2M cacodylate  
424 buffer. Mice were euthanized and eyes with optic nerves were post fixed in half Karnovsky's  
425 fixative. Tissues were placed in 2% glutaraldehyde overnight and then rinsed in 0.1M phosphate  
426 buffer with osmium tetroxide. Osmicated tissues were rinsed in 0.15M phosphate buffer and  
427 dehydrated with graded concentrations of cold ethanol, ranging from 25 to 100%. Dehydrated  
428 tissues were rinsed with propylene oxide and embedded in Epon-Araldite with DMP-30 (All  
429 reagents were purchased from Electron Microscopy Sciences). Mitochondrial numbers were  
430 counted per axon area delineated by morphological features. Mitochondrial and axon boundaries  
431 were manually traced, and the areas were calculated using ImageJ analysis software (National  
432 Institutes of Health).

433  
434 **Mitochondrial Purification.** Whole retinas or optic nerves and tracts were quickly dissected from  
435 CO<sub>2</sub> sacrificed mice, and homogenized using a dounce tissue grinder (Wheaton, 357538) with 20-

436 30 strokes in mitochondrial isolation buffer (provided in the Mitochondria Isolation Kit, Miltenyi  
437 Biotec, 130-096-946) with protease inhibitors (ThermoFisher Scientific, 78425). The homogenate  
438 was then spun at 1000g and the supernatant was removed for subsequent magnet based  
439 mitochondrial isolation according to Miltenyi Biotec's Mitochondrial Isolation Kit. Isolated  
440 mitochondria were washed and re-pelleted three times to insure mitochondrial fractions were pure  
441 and intact, for all downstream experiments. In addition, all procedures were performed on ice or  
442 at 4°C, to preserve mitochondrial integrity.

443  
444 **FACS analyses of mitochondria.** CFP-expressing mitochondria were analyzed with forward and  
445 side scatter in a Becton Dickinson FACScan (Becton Dickinson, San Jose, CA). Data were  
446 acquired in list mode, evaluated with WinList software (Verity Software House). In some  
447 experiments, mitochondria were detected with anti-TOM20 antibodies (Abcam, ab78547) or  
448 mitotracker CMXROS (ThermoFisher Scientific, M7512). To determine if mitochondria were  
449 intact and viable, FACS sorted mitochondria were equilibrated with the membrane potential-  
450 sensitive dye JC-1 (500 nM; 5,5',6,6-tetra-chloro-1,1,3,3-tetraethylbenzimidazol-carbocyanine  
451 iodide; ThermoFisher Scientific, T3168) for 20 minutes with or without FCCP (10 µM;  
452 carbonylcyanide-P-trifluoromethoxyphenylhydrazine; Sigma Aldrich, C2920).

453  
454 **Western Blots.** To further evaluate the structural integrity and purity of isolated mitochondria,  
455 mitochondria were analyzed by western blot using the following antibodies. Antibodies against  
456 inner and outer mitochondrial membrane integrity proteins include; Outer Membrane - Porin  
457 (VDAC1), Inner Membrane - Ubiquinol Cytochrome C Reductase Core Protein I, Intermembrane  
458 Space - Cytochrome C and Complex Va, and Matrix Space-Cyclophilin 40, (Abcam-ab110414;

459 ab14734, ab110252, ab110325, ab110273, and ab110324). Electron transport chain protein  
460 antibodies include; Complex I subunit (NDUFB8), Complex II-30kDa (SH3B), Complex III-Core  
461 Protein 2 (UQCRC2), Complex IV subunit I (MTCO1), and Complex V alpha subunit (ATP5A)  
462 (Abcam-ab1104; ab110242, ab14714, ab14745, ab14705, and ab14748). Cytoplasmic antibodies  
463 include; GAPDH and  $\beta$ -Actin (Cell Signaling Technology, 2118S and 8457). GFP/CFP antibodies  
464 (Thermofisher Scientific, A10262) were used as controls for the integrity of mitochondrial  
465 fractions collected from Thy1-CFP/COX8A mice.

466  
467 **Proteomics.** To detect mitochondrial associated proteins, mitochondrial purification was  
468 performed on 24 optic nerves and 6 retinas. Resulting mitochondrial pellets were solubilized with  
469 5% rapigest in TNE buffer and then boiled for 5 min, followed by reduction in 1mM Tris(2-  
470 carboxyethyl)phosphine hydrochloride at 37°C for 30min. Then samples were alkylated in .5mM  
471 2-iodoacetamide at 37°C for 30min, followed by trypsin digestions at 1:50 (enzyme:protein)  
472 overnight at 37°C and the addition of 250mM HCl at 37°C for 1hr. Samples were then centrifuged  
473 and peptides were extracted from the supernatant and desalted using Aspire RP30 desalting  
474 columns (Thermo Scientific)<sup>95</sup>. Trypsin-digested peptides were analyzed by LC-MS/MS<sup>96</sup> on the  
475 TripleTOF™ 5600 hybrid mass spectrometer (ABSCIEX). MS/MS data were acquired in a data-  
476 dependent manner in which the MS1 data was acquired for 250 ms at m/z of 400 to 1250 Da and  
477 the MS/MS data was acquired from m/z of 50 to 2,000 Da. For Independent data acquisition (IDA)  
478 parameters MS1-TOF 250 milliseconds, followed by 50 MS2 events of 25 milliseconds each. The  
479 IDA criteria; over 200 counts threshold, charge state of plus 2-4 with 4 seconds exclusion window.  
480 Finally, the collected data were analyzed and normalized<sup>97</sup> using MASCOT® (Matrix Sciences)  
481 and Protein Pilot 4.0 (ABSCIEX) for peptide identifications normalized based on spectral

482 abundance factors.

483

484 **RNA detection.** To detect mitochondrial or nuclear-encoded mRNA transcripts, RNA was  
485 extracted from isolated RGCs or mitochondria from retina or optic nerve and tract using the  
486 RNeasy Plus Micro Kit (Qiagen, 74034). RNA isolates were then processed for RT<sup>2</sup> Profiler™  
487 PCR Arrays (Mouse Mitochondrial and Mitochondria Energy Metabolism, PAMM-087ZE and  
488 PAMM-008ZE). For mitochondrial RNA release assays, isolated mitochondria were resuspended  
489 in mitochondrial suspension buffer (provided in Mitochondria Isolation Kit) and incubated with  
490 Proteinase K (Thermofisher Scientific, 25530049) at 5ug/mL for 10 min. Mitochondria were then  
491 pelleted, and supernatant and mitochondrial pellets were separately processed for RNA  
492 purification and subsequent qPCR arrays. All qPCR data were acquired on QuantStudio 7 Flex  
493 Real-Time PCR System (Applied Biosystems, Thermofisher Scientific).

494

495 **Pharmacologic interventions.** Mice were anesthetized with xylazine (10 mg/kg, IP) and ketamine  
496 (80 mg/kg, IP). Anesthetized mice were injected intravitreally (1-2 µl) with vehicle, Hank's  
497 balanced salt solution (HBS, Invitrogen), BDNF (3µg/µl; Peprotech #450-02), tetrodotoxin (TTX;  
498 3 µM, Sigma #T8024), or combined TTX (3 µM) and BDNF (3.3 µg/µl; Peprotech).

499

500 **Eyelid opening or suturing.** For premature eyelid opening experiments, P10 mice were  
501 anesthetized as above and eyelids were gently pried open with forceps as described<sup>98</sup>. Eyes were  
502 then treated with sterile 2.5% hydroxypropyl methylcellulose (Goniosol, Akorn) every 12-18 hours  
503 to ensure eyes remained open and lubricated throughout the duration of the experiment. For  
504 extended eyelid closure experiments, P11 pups were anesthetized and two mattress sutures were

505 placed along the eyelid margin to prevent eye opening as described<sup>99</sup>. Animals were checked daily  
506 to ensure sutured eyes remained closed until euthanasia.

507

508 **Graphing and Statistics.** Data presentation and statistical analysis was done in Prism (Graphpad).

509 To compare quantitative variables, Student's t-tests or ANOVA with post-hoc t-tests were done  
510 with a  $p$ -value < 0.05 indicating statistical significance.

511

## 512 **Acknowledgements**

513

514 We gratefully acknowledge funding from the NIH R01-EY020913 (JLG), P30-EY014801  
515 (University of Miami), P30-EY026877 (Stanford University), F31-NS087789 (AK), as well as  
516 unrestricted grants from Research to Prevent Blindness, Inc. We thank the following for their  
517 technical support; Peggy Bates for electron microscopy, George McNamara and Gabe Gaidosh for  
518 microscopy, Kristina Russano and Eleut Hernandez for animal husbandry, Oliver Umland for  
519 assistance in flow cytometry, and Majid Ghassemian for mass spectrometry support.

520

521 **Competing interests:** The authors declare that no competing interests exist.

522

## 523 **References**

524 1 Wong-Riley, M. T. Energy metabolism of the visual system. *Eye Brain* **2**, 99-116,  
525 doi:10.2147/EB.S9078 (2010).

526 2 Agathocleous, M. *et al.* Metabolic differentiation in the embryonic retina. *Nat Cell Biol* **14**,  
527 859-864, doi:10.1038/ncb2531 (2012).

- 528 3 Agostini, M. *et al.* Metabolic reprogramming during neuronal differentiation. *Cell Death*  
529 *Differ* **23**, 1502-1514, doi:10.1038/cdd.2016.36 (2016).
- 530 4 Kann, O. & Kovacs, R. Mitochondria and neuronal activity. *American journal of*  
531 *physiology. Cell physiology* **292**, C641-657, doi:10.1152/ajpcell.00222.2006 (2007).
- 532 5 Johnson, D. T. *et al.* Tissue heterogeneity of the mammalian mitochondrial proteome.  
533 *American journal of physiology. Cell physiology* **292**, C689-697,  
534 doi:10.1152/ajpcell.00108.2006 (2007).
- 535 6 Gaston, D., Tsaousis, A. D. & Roger, A. J. Predicting proteomes of mitochondria and  
536 related organelles from genomic and expressed sequence tag data. *Methods Enzymol* **457**,  
537 21-47, doi:10.1016/S0076-6879(09)05002-2 (2009).
- 538 7 Mootha, V. K. *et al.* Integrated analysis of protein composition, tissue diversity, and gene  
539 regulation in mouse mitochondria. *Cell* **115**, 629-640 (2003).
- 540 8 Pagliarini, D. J. *et al.* A mitochondrial protein compendium elucidates complex I disease  
541 biology. *Cell* **134**, 112-123, doi:10.1016/j.cell.2008.06.016 (2008).
- 542 9 Sickmann, A. *et al.* The proteome of *Saccharomyces cerevisiae* mitochondria. *Proc Natl*  
543 *Acad Sci U S A* **100**, 13207-13212, doi:10.1073/pnas.2135385100 (2003).
- 544 10 Calvo, S. E., Clauser, K. R. & Mootha, V. K. MitoCarta2.0: an updated inventory of  
545 mammalian mitochondrial proteins. *Nucleic Acids Res* **44**, D1251-1257,  
546 doi:10.1093/nar/gkv1003 (2016).
- 547 11 Anderson, S. *et al.* Sequence and organization of the human mitochondrial genome. *Nature*  
548 **290**, 457-465 (1981).
- 549 12 Kurland, C. G. & Andersson, S. G. Origin and evolution of the mitochondrial proteome.  
550 *Microbiology and molecular biology reviews : MMBR* **64**, 786-820 (2000).



- 551 13 Zhou, B. *et al.* Facilitation of axon regeneration by enhancing mitochondrial transport and  
552 rescuing energy deficits. *J Cell Biol* **214**, 103-119, doi:10.1083/jcb.201605101 (2016).
- 553 14 Ryan, M. T. & Hoogenraad, N. J. Mitochondrial-nuclear communications. *Annu Rev*  
554 *Biochem* **76**, 701-722, doi:10.1146/annurev.biochem.76.052305.091720 (2007).
- 555 15 Varadi, A. *et al.* Cytoplasmic dynein regulates the subcellular distribution of mitochondria  
556 by controlling the recruitment of the fission factor dynamin-related protein-1. *J Cell Sci*  
557 **117**, 4389-4400, doi:10.1242/jcs.01299 (2004).
- 558 16 Hancock, W. O. Bidirectional cargo transport: moving beyond tug of war. *Nat Rev Mol*  
559 *Cell Biol* **15**, 615-628, doi:10.1038/nrm3853 (2014).
- 560 17 Stuart, R. A., Cyr, D. M., Craig, E. A. & Neupert, W. Mitochondrial molecular chaperones:  
561 their role in protein translocation. *Trends Biochem Sci* **19**, 87-92, doi:10.1016/0968-  
562 0004(94)90041-8 (1994).
- 563 18 Sheng, Z. H. & Cai, Q. Mitochondrial transport in neurons: impact on synaptic homeostasis  
564 and neurodegeneration. *Nat Rev Neurosci* **13**, 77-93, doi:10.1038/nrn3156 (2012).
- 565 19 Youle, R. J. & van der Bliek, A. M. Mitochondrial fission, fusion, and stress. *Science* **337**,  
566 1062-1065, doi:10.1126/science.1219855 (2012).
- 567 20 Amiri, M. & Hollenbeck, P. J. Mitochondrial biogenesis in the axons of vertebrate  
568 peripheral neurons. *Dev Neurobiol* **68**, 1348-1361, doi:10.1002/dneu.20668 (2008).
- 569 21 Mattson, M. P., Gleichmann, M. & Cheng, A. Mitochondria in neuroplasticity and  
570 neurological disorders. *Neuron* **60**, 748-766, doi:10.1016/j.neuron.2008.10.010 (2008).
- 571 22 Van Laar, V. S. *et al.* Evidence for compartmentalized axonal mitochondrial biogenesis:  
572 Mitochondrial DNA replication increases in distal axons as an early response to Parkinson's  
573 disease-relevant stress. *J Neurosci*, doi:10.1523/JNEUROSCI.0541-18.2018 (2018).

- 574 23 Jung, H., Yoon, B. C. & Holt, C. E. Axonal mRNA localization and local protein synthesis  
575 in nervous system assembly, maintenance and repair. *Nat Rev Neurosci* **13**, 308-324,  
576 doi:10.1038/nrn3210 (2012).
- 577 24 Gioio, A. E. *et al.* Local synthesis of nuclear-encoded mitochondrial proteins in the  
578 presynaptic nerve terminal. *Journal of neuroscience research* **64**, 447-453 (2001).
- 579 25 Aschrafi, A., Natera-Naranjo, O., Gioio, A. E. & Kaplan, B. B. Regulation of axonal  
580 trafficking of cytochrome c oxidase IV mRNA. *Mol Cell Neurosci* **43**, 422-430,  
581 doi:10.1016/j.mcn.2010.01.009 (2010).
- 582 26 Hillefors, M., Gioio, A. E., Mameza, M. G. & Kaplan, B. B. Axon viability and  
583 mitochondrial function are dependent on local protein synthesis in sympathetic neurons.  
584 *Cell Mol Neurobiol* **27**, 701-716, doi:10.1007/s10571-007-9148-y (2007).
- 585 27 Shigeoka, T. *et al.* Dynamic Axonal Translation in Developing and Mature Visual Circuits.  
586 *Cell* **166**, 181-192, doi:10.1016/j.cell.2016.05.029 (2016).
- 587 28 Mercer, T. R. *et al.* The human mitochondrial transcriptome. *Cell* **146**, 645-658,  
588 doi:10.1016/j.cell.2011.06.051 (2011).
- 589 29 Gehrke, S. *et al.* PINK1 and Parkin control localized translation of respiratory chain  
590 component mRNAs on mitochondria outer membrane. *Cell Metab* **21**, 95-108,  
591 doi:10.1016/j.cmet.2014.12.007 (2015).
- 592 30 Matsumoto, S. *et al.* Localization of mRNAs encoding human mitochondrial oxidative  
593 phosphorylation proteins. *Mitochondrion* **12**, 391-398, doi:10.1016/j.mito.2012.02.004  
594 (2012).
- 595 31 Wong, H. H. *et al.* RNA Docking and Local Translation Regulate Site-Specific Axon  
596 Remodeling In Vivo. *Neuron* **95**, 852-868 e858, doi:10.1016/j.neuron.2017.07.016 (2017).

- 597 32 Kaewsapsak, P., Shechner, D. M., Mallard, W., Rinn, J. L. & Ting, A. Y. Live-cell mapping  
598 of organelle-associated RNAs via proximity biotinylation combined with protein-RNA  
599 crosslinking. *Elife* **6**, doi:10.7554/eLife.29224 (2017).
- 600 33 Kellems, R. E., Allison, V. F. & Butow, R. A. Cytoplasmic type 80S ribosomes associated  
601 with yeast mitochondria. IV. Attachment of ribosomes to the outer membrane of isolated  
602 mitochondria. *J Cell Biol* **65**, 1-14 (1975).
- 603 34 Crowley, K. S. & Payne, R. M. Ribosome binding to mitochondria is regulated by GTP  
604 and the transit peptide. *J Biol Chem* **273**, 17278-17285 (1998).
- 605 35 Williams, C. C., Jan, C. H. & Weissman, J. S. Targeting and plasticity of mitochondrial  
606 proteins revealed by proximity-specific ribosome profiling. *Science* **346**, 748-751,  
607 doi:10.1126/science.1257522 (2014).
- 608 36 Majdan, M. & Shatz, C. J. Effects of visual experience on activity-dependent gene  
609 regulation in cortex. *Nat Neurosci* **9**, 650-659, doi:10.1038/nm1674 (2006).
- 610 37 Tian, N. & Copenhagen, D. R. Visual stimulation is required for refinement of ON and  
611 OFF pathways in postnatal retina. *Neuron* **39**, 85-96 (2003).
- 612 38 Feller, M. B. Retinal waves are likely to instruct the formation of eye-specific  
613 retinogeniculate projections. *Neural development* **4**, 24, doi:10.1186/1749-8104-4-24  
614 (2009).
- 615 39 Reese, B. E. Development of the retina and optic pathway. *Vision research* **51**, 613-632,  
616 doi:10.1016/j.visres.2010.07.010 (2011).
- 617 40 Chandrasekaran, A. R., Plas, D. T., Gonzalez, E. & Crair, M. C. Evidence for an instructive  
618 role of retinal activity in retinotopic map refinement in the superior colliculus of the mouse.  
619 *J Neurosci* **25**, 6929-6938, doi:10.1523/JNEUROSCI.1470-05.2005 (2005).

- 620 41 Feller, M. B., Wellis, D. P., Stellwagen, D., Werblin, F. S. & Shatz, C. J. Requirement for  
621 cholinergic synaptic transmission in the propagation of spontaneous retinal waves. *Science*  
622 **272**, 1182-1187 (1996).
- 623 42 Akerman, C. J., Smyth, D. & Thompson, I. D. Visual experience before eye-opening and  
624 the development of the retinogeniculate pathway. *Neuron* **36**, 869-879 (2002).
- 625 43 Huberman, A. D. *et al.* Eye-specific retinogeniculate segregation independent of normal  
626 neuronal activity. *Science* **300**, 994-998, doi:10.1126/science.1080694 (2003).
- 627 44 Etxeberria, A. *et al.* Dynamic Modulation of Myelination in Response to Visual Stimuli  
628 Alters Optic Nerve Conduction Velocity. *J Neurosci* **36**, 6937-6948,  
629 doi:10.1523/JNEUROSCI.0908-16.2016 (2016).
- 630 45 Young, R. W. Cell death during differentiation of the retina in the mouse. *J Comp Neurol*  
631 **229**, 362-373, doi:10.1002/cne.902290307 (1984).
- 632 46 Galli-Resta, L. & Ensini, M. An intrinsic time limit between genesis and death of individual  
633 neurons in the developing retinal ganglion cell layer. *J Neurosci* **16**, 2318-2324 (1996).
- 634 47 Beros, J., Rodger, J. & Harvey, A. R. Developmental retinal ganglion cell death and  
635 retinotopicity of the murine retinocollicular projection. *Dev Neurobiol*,  
636 doi:10.1002/dneu.22559 (2017).
- 637 48 Frank, S. *et al.* The role of dynamin-related protein 1, a mediator of mitochondrial fission,  
638 in apoptosis. *Developmental cell* **1**, 515-525 (2001).
- 639 49 Estaquier, J. & Arnoult, D. Inhibiting Drp1-mediated mitochondrial fission selectively  
640 prevents the release of cytochrome c during apoptosis. *Cell Death Differ* **14**, 1086-1094,  
641 doi:10.1038/sj.cdd.4402107 (2007).

- 642 50 Liu, C. J., Chaturvedi, N., Barnstable, C. J. & Dreyer, E. B. Retinal Thy-1 expression  
643 during development. *Invest Ophthalmol Vis Sci* **37**, 1469-1473 (1996).
- 644 51 Mojumder, D. K., Sherry, D. M. & Frishman, L. J. Contribution of voltage-gated sodium  
645 channels to the b-wave of the mammalian flash electroretinogram. *The Journal of*  
646 *physiology* **586**, 2551-2580, doi:10.1113/jphysiol.2008.150755 (2008).
- 647 52 Seki, M., Nawa, H., Fukuchi, T., Abe, H. & Takei, N. BDNF is upregulated by postnatal  
648 development and visual experience: quantitative and immunohistochemical analyses of  
649 BDNF in the rat retina. *Investigative ophthalmology & visual science* **44**, 3211-3218  
650 (2003).
- 651 53 Markham, A., Cameron, I., Franklin, P. & Spedding, M. BDNF increases rat brain  
652 mitochondrial respiratory coupling at complex I, but not complex II. *Eur J Neurosci* **20**,  
653 1189-1196, doi:10.1111/j.1460-9568.2004.03578.x (2004).
- 654 54 Su, B., Ji, Y. S., Sun, X. L., Liu, X. H. & Chen, Z. Y. Brain-derived neurotrophic factor  
655 (BDNF)-induced mitochondrial motility arrest and presynaptic docking contribute to  
656 BDNF-enhanced synaptic transmission. *J Biol Chem* **289**, 1213-1226,  
657 doi:10.1074/jbc.M113.526129 (2014).
- 658 55 Guo, J. *et al.* BDNF pro-peptide regulates dendritic spines via caspase-3. *Cell Death Dis*  
659 **7**, e2264, doi:10.1038/cddis.2016.166 (2016).
- 660 56 Jao, C. Y. & Salic, A. Exploring RNA transcription and turnover in vivo by using click  
661 chemistry. *Proc Natl Acad Sci U S A* **105**, 15779-15784, doi:10.1073/pnas.0808480105  
662 (2008).

- 663 57 Liu, J., Xu, Y., Stoleru, D. & Salic, A. Imaging protein synthesis in cells and tissues with  
664 an alkyne analog of puromycin. *Proc Natl Acad Sci U S A* **109**, 413-418,  
665 doi:10.1073/pnas.1111561108 (2012).
- 666 58 Lipton, S. A. Blockade of electrical activity promotes the death of mammalian retinal  
667 ganglion cells in culture. *Proc Natl Acad Sci U S A* **83**, 9774-9778 (1986).
- 668 59 Griffin, J. W., Price, D. L., Drachman, D. B. & Engel, W. K. Axonal transport to and from  
669 the motor nerve ending. *Ann N Y Acad Sci* **274**, 31-45 (1976).
- 670 60 Goldberg, J. L., Klassen, M. P., Hua, Y. & Barres, B. A. Amacrine-signaled loss of intrinsic  
671 axon growth ability by retinal ganglion cells. *Science* **296**, 1860-1864,  
672 doi:10.1126/science.1068428 (2002).
- 673 61 Graifer, D., Malygin, A., Zharkov, D. O. & Karpova, G. Eukaryotic ribosomal protein S3:  
674 A constituent of translational machinery and an extraribosomal player in various cellular  
675 processes. *Biochimie* **99**, 8-18, doi:10.1016/j.biochi.2013.11.001 (2014).
- 676 62 Franko, A. *et al.* Efficient isolation of pure and functional mitochondria from mouse tissues  
677 using automated tissue disruption and enrichment with anti-TOM22 magnetic beads. *PLoS*  
678 *One* **8**, e82392, doi:10.1371/journal.pone.0082392 (2013).
- 679 63 Huang da, W., Sherman, B. T. & Lempicki, R. A. Systematic and integrative analysis of  
680 large gene lists using DAVID bioinformatics resources. *Nat Protoc* **4**, 44-57,  
681 doi:10.1038/nprot.2008.211 (2009).
- 682 64 Thomas, P. D. *et al.* PANTHER: a library of protein families and subfamilies indexed by  
683 function. *Genome Res* **13**, 2129-2141, doi:10.1101/gr.772403 (2003).

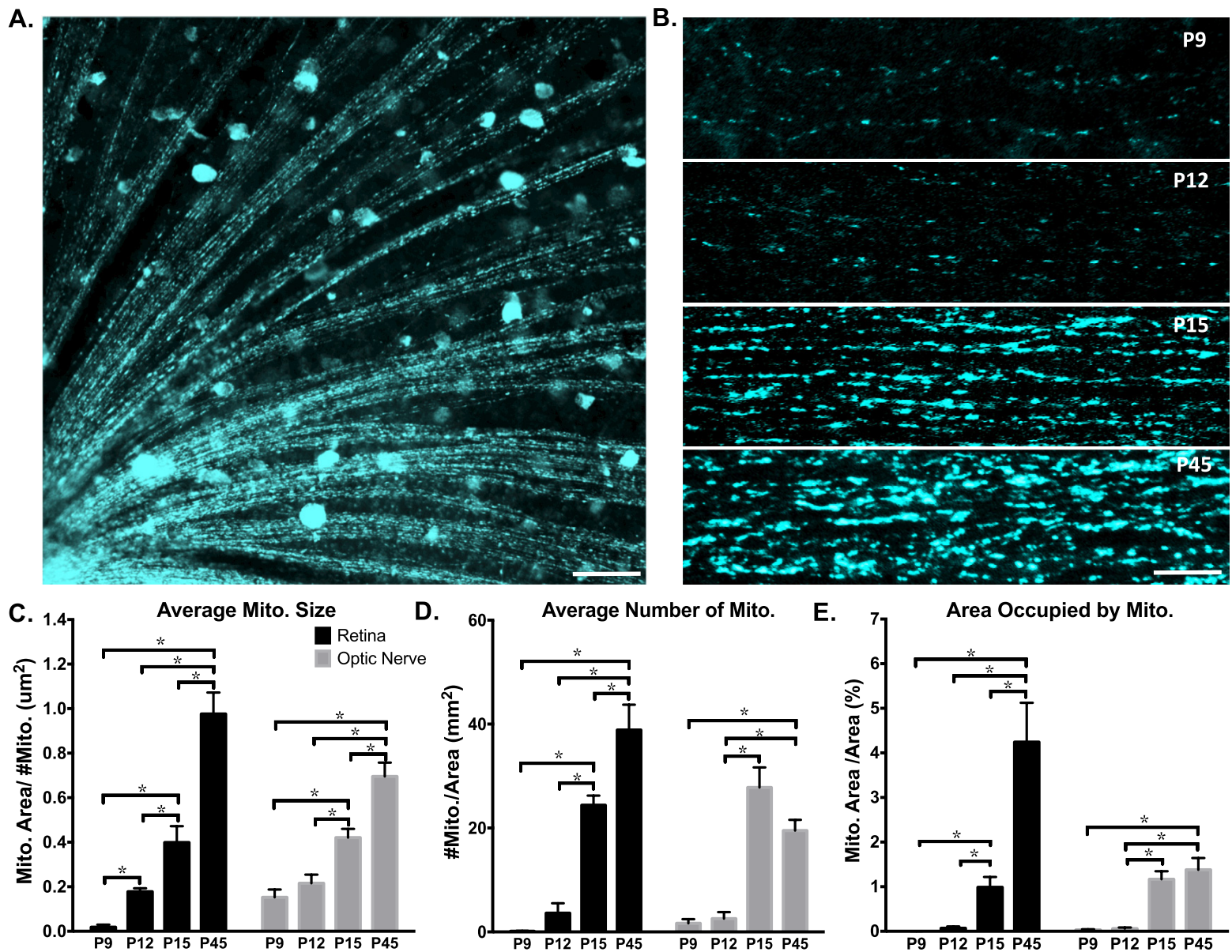
- 684 65 Pundir, S., Magrane, M., Martin, M. J., O'Donovan, C. & UniProt, C. Searching and  
685 Navigating UniProt Databases. *Curr Protoc Bioinformatics* **50**, 1 27 21-10,  
686 doi:10.1002/0471250953.bi0127s50 (2015).
- 687 66 Liao, Y. *et al.* The Cardiomyocyte RNA-Binding Proteome: Links to Intermediary  
688 Metabolism and Heart Disease. *Cell Rep* **16**, 1456-1469, doi:10.1016/j.celrep.2016.06.084  
689 (2016).
- 690 67 Baltz, A. G. *et al.* The mRNA-bound proteome and its global occupancy profile on protein-  
691 coding transcripts. *Mol Cell* **46**, 674-690, doi:10.1016/j.molcel.2012.05.021 (2012).
- 692 68 Castello, A. *et al.* Insights into RNA biology from an atlas of mammalian mRNA-binding  
693 proteins. *Cell* **149**, 1393-1406, doi:10.1016/j.cell.2012.04.031 (2012).
- 694 69 Giudice, G., Sanchez-Cabo, F., Torroja, C. & Lara-Pezzi, E. ATtRACT-a database of  
695 RNA-binding proteins and associated motifs. *Database (Oxford)* **2016**,  
696 doi:10.1093/database/baw035 (2016).
- 697 70 Cook, K. B., Kazan, H., Zuberi, K., Morris, Q. & Hughes, T. R. RBPDB: a database of  
698 RNA-binding specificities. *Nucleic Acids Res* **39**, D301-308, doi:10.1093/nar/gkq1069  
699 (2011).
- 700 71 Gerstberger, S., Hafner, M. & Tuschl, T. A census of human RNA-binding proteins. *Nat*  
701 *Rev Genet* **15**, 829-845, doi:10.1038/nrg3813 (2014).
- 702 72 Castello, A. *et al.* Comprehensive Identification of RNA-Binding Domains in Human  
703 Cells. *Mol Cell* **63**, 696-710, doi:10.1016/j.molcel.2016.06.029 (2016).
- 704 73 Shieh, P. B., Hu, S. C., Bobb, K., Timmusk, T. & Ghosh, A. Identification of a signaling  
705 pathway involved in calcium regulation of BDNF expression. *Neuron* **20**, 727-740 (1998).

- 706 74 Lein, E. S., Hohn, A. & Shatz, C. J. Dynamic regulation of BDNF and NT-3 expression  
707 during visual system development. *The Journal of comparative neurology* **420**, 1-18  
708 (2000).
- 709 75 Lu, B. BDNF and activity-dependent synaptic modulation. *Learning & memory* **10**, 86-98,  
710 doi:10.1101/lm.54603 (2003).
- 711 76 Marosi, K. & Mattson, M. P. BDNF mediates adaptive brain and body responses to  
712 energetic challenges. *Trends Endocrinol Metab* **25**, 89-98, doi:10.1016/j.tem.2013.10.006  
713 (2014).
- 714 77 Camandola, S. & Mattson, M. P. Brain metabolism in health, aging, and  
715 neurodegeneration. *EMBO J* **36**, 1474-1492, doi:10.15252/emj.201695810 (2017).
- 716 78 Wareski, P. *et al.* PGC-1 $\{\alpha\}$  and PGC-1 $\{\beta\}$  regulate mitochondrial density in  
717 neurons. *J Biol Chem* **284**, 21379-21385, doi:10.1074/jbc.M109.018911 (2009).
- 718 79 Schieke, S. M. *et al.* The mammalian target of rapamycin (mTOR) pathway regulates  
719 mitochondrial oxygen consumption and oxidative capacity. *J Biol Chem* **281**, 27643-  
720 27652, doi:10.1074/jbc.M603536200 (2006).
- 721 80 Divakaruni, A. S., Paradyse, A., Ferrick, D. A., Murphy, A. N. & Jastroch, M. Analysis  
722 and interpretation of microplate-based oxygen consumption and pH data. *Methods*  
723 *Enzymol* **547**, 309-354, doi:10.1016/B978-0-12-801415-8.00016-3 (2014).
- 724 81 Burkhalter, J., Fiumelli, H., Allaman, I., Chatton, J. Y. & Martin, J. L. Brain-derived  
725 neurotrophic factor stimulates energy metabolism in developing cortical neurons. *J*  
726 *Neurosci* **23**, 8212-8220 (2003).
- 727 82 Chan, S. L. & Quastel, J. H. Tetrodotoxin: effects on brain metabolism in vitro. *Science*  
728 **156**, 1752-1753 (1967).

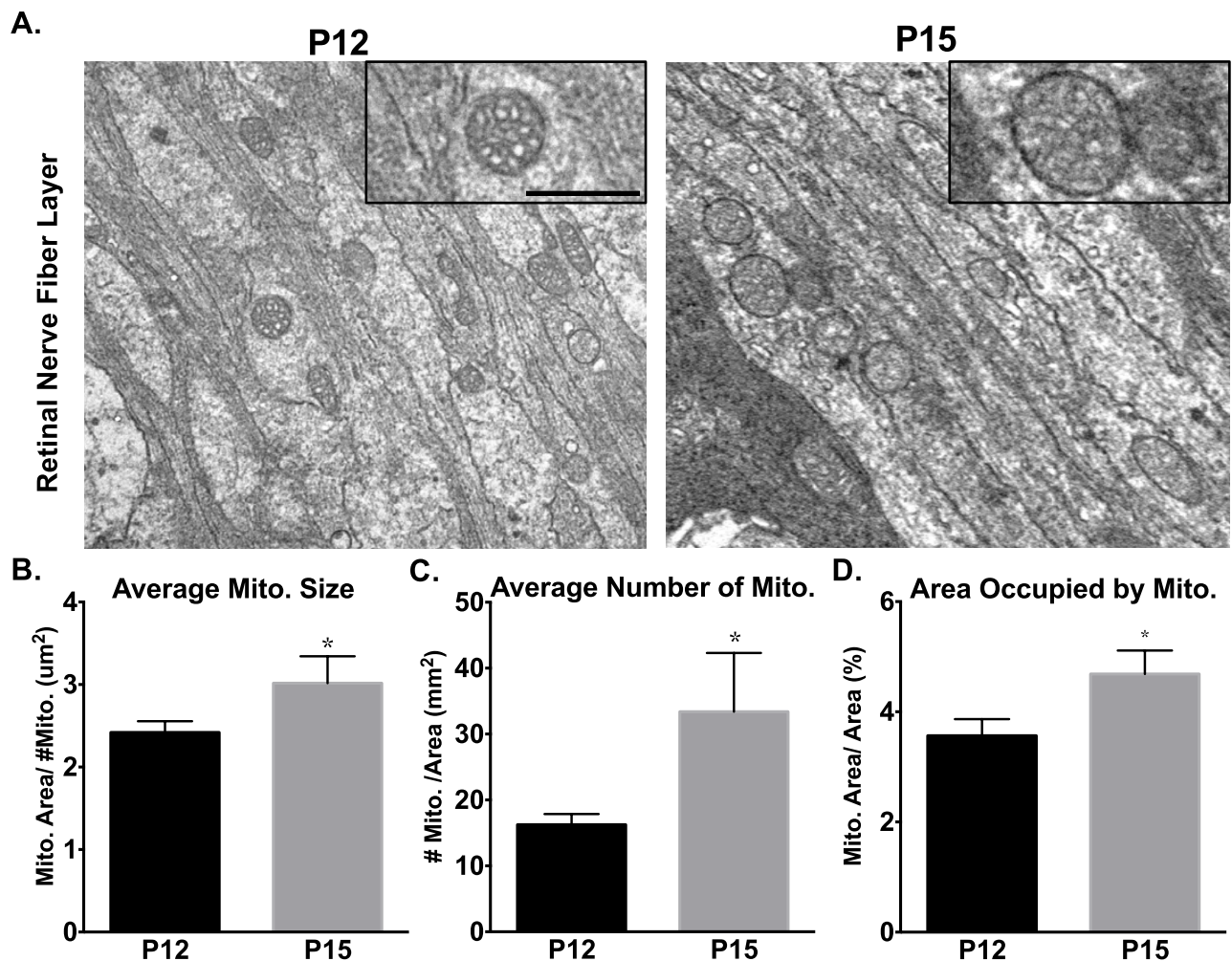


- 729 83 Smith, R. S. The short term accumulation of axonally transported organelles in the region  
730 of localized lesions of single myelinated axons. *J Neurocytol* **9**, 39-65 (1980).
- 731 84 Tsukita, S. & Ishikawa, H. The movement of membranous organelles in axons. Electron  
732 microscopic identification of anterogradely and retrogradely transported organelles. *J Cell*  
733 *Biol* **84**, 513-530 (1980).
- 734 85 Yao, J., Sasaki, Y., Wen, Z., Bassell, G. J. & Zheng, J. Q. An essential role for beta-actin  
735 mRNA localization and translation in Ca<sup>2+</sup>-dependent growth cone guidance. *Nat*  
736 *Neurosci* **9**, 1265-1273, doi:10.1038/nm1773 (2006).
- 737 86 Leung, K. M. *et al.* Asymmetrical beta-actin mRNA translation in growth cones mediates  
738 attractive turning to netrin-1. *Nat Neurosci* **9**, 1247-1256, doi:10.1038/nm1775 (2006).
- 739 87 Lin, M. T. & Beal, M. F. Mitochondrial dysfunction and oxidative stress in  
740 neurodegenerative diseases. *Nature* **443**, 787-795, doi:10.1038/nature05292 (2006).
- 741 88 Alami, N. H. *et al.* Axonal transport of TDP-43 mRNA granules is impaired by ALS-  
742 causing mutations. *Neuron* **81**, 536-543, doi:10.1016/j.neuron.2013.12.018 (2014).
- 743 89 Lemmens, R., Moore, M. J., Al-Chalabi, A., Brown, R. H., Jr. & Robberecht, W. RNA  
744 metabolism and the pathogenesis of motor neuron diseases. *Trends Neurosci* **33**, 249-258,  
745 doi:10.1016/j.tins.2010.02.003 (2010).
- 746 90 Rossor, A. M., Kalmar, B., Greensmith, L. & Reilly, M. M. The distal hereditary motor  
747 neuropathies. *J Neurol Neurosurg Psychiatry* **83**, 6-14, doi:10.1136/jnnp-2011-300952  
748 (2012).
- 749 91 Zahn, J. M. *et al.* AGEMAP: a gene expression database for aging in mice. *PLoS genetics*  
750 **3**, e201, doi:10.1371/journal.pgen.0030201 (2007).

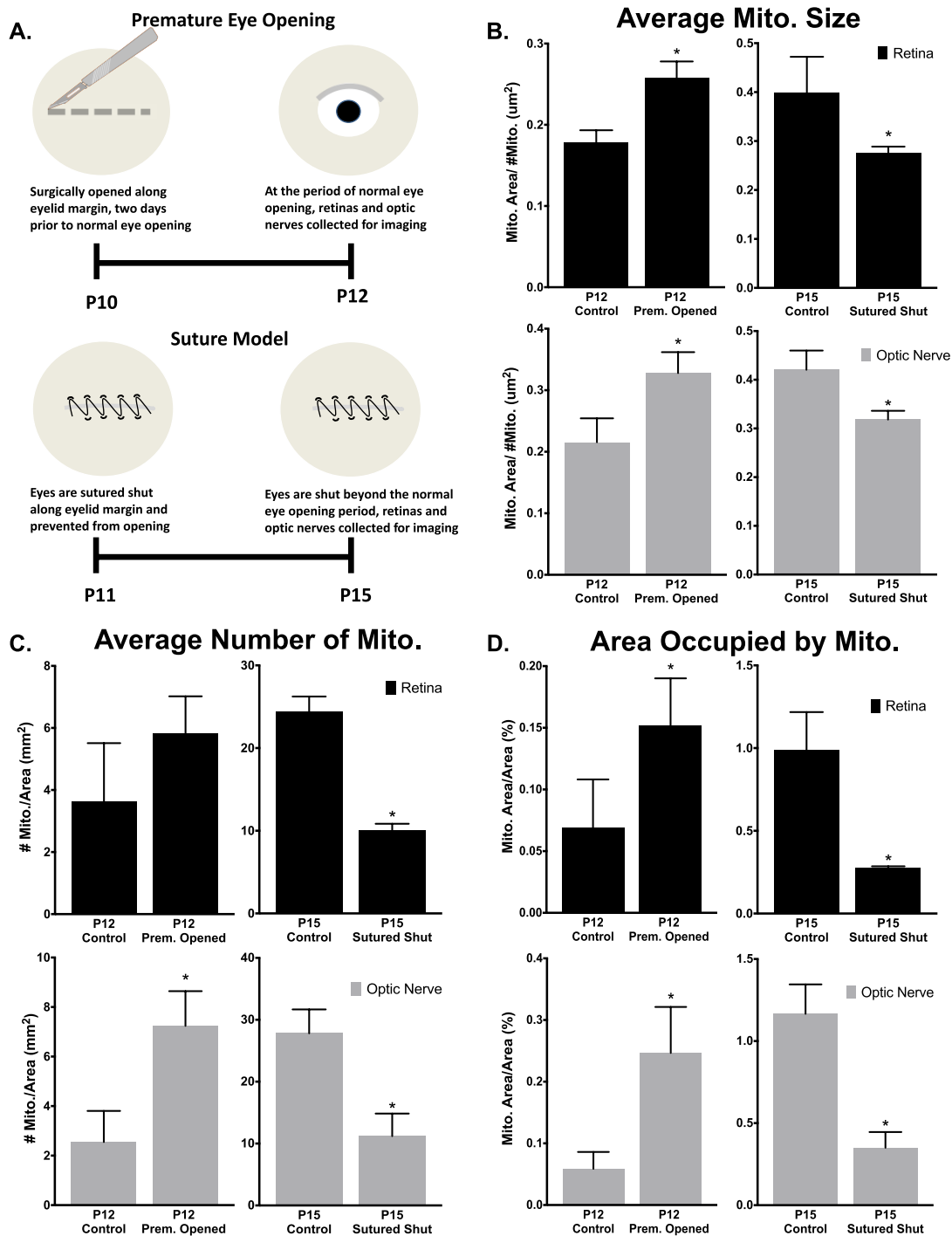
- 751 92 Blalock, E. M. *et al.* Gene microarrays in hippocampal aging: statistical profiling identifies  
752 novel processes correlated with cognitive impairment. *J Neurosci* **23**, 3807-3819 (2003).
- 753 93 Steketee, M. B. *et al.* Mitochondrial dynamics regulate growth cone motility, guidance,  
754 and neurite growth rate in perinatal retinal ganglion cells in vitro. *Invest Ophthalmol Vis*  
755 *Sci* **53**, 7402-7411, doi:10.1167/iovs.12-10298 (2012).
- 756 94 Barres, B. A., Silverstein, B. E., Corey, D. P. & Chun, L. L. Immunological,  
757 morphological, and electrophysiological variation among retinal ganglion cells purified by  
758 panning. *Neuron* **1**, 791-803 (1988).
- 759 95 Guttman, M. *et al.* Interactions of the NPXY microdomains of the low density lipoprotein  
760 receptor-related protein 1. *Proteomics* **9**, 5016-5028, doi:10.1002/pmic.200900457 (2009).
- 761 96 McCormack, A. L. *et al.* Direct analysis and identification of proteins in mixtures by  
762 LC/MS/MS and database searching at the low-femtomole level. *Anal Chem* **69**, 767-776  
763 (1997).
- 764 97 Paoletti, A. C. *et al.* Quantitative proteomic analysis of distinct mammalian Mediator  
765 complexes using normalized spectral abundance factors. *Proc Natl Acad Sci U S A* **103**,  
766 18928-18933, doi:10.1073/pnas.0606379103 (2006).
- 767 98 Watanabe, H., Tisdale, A. S. & Gipson, I. K. Eyelid opening induces expression of a  
768 glycoalyx glycoprotein of rat ocular surface epithelium. *Investigative ophthalmology &*  
769 *visual science* **34**, 327-338 (1993).
- 770 99 Gordon, J. A. & Stryker, M. P. Experience-dependent plasticity of binocular responses in  
771 the primary visual cortex of the mouse. *The Journal of neuroscience : the official journal*  
772 *of the Society for Neuroscience* **16**, 3274-3286 (1996).
- 773



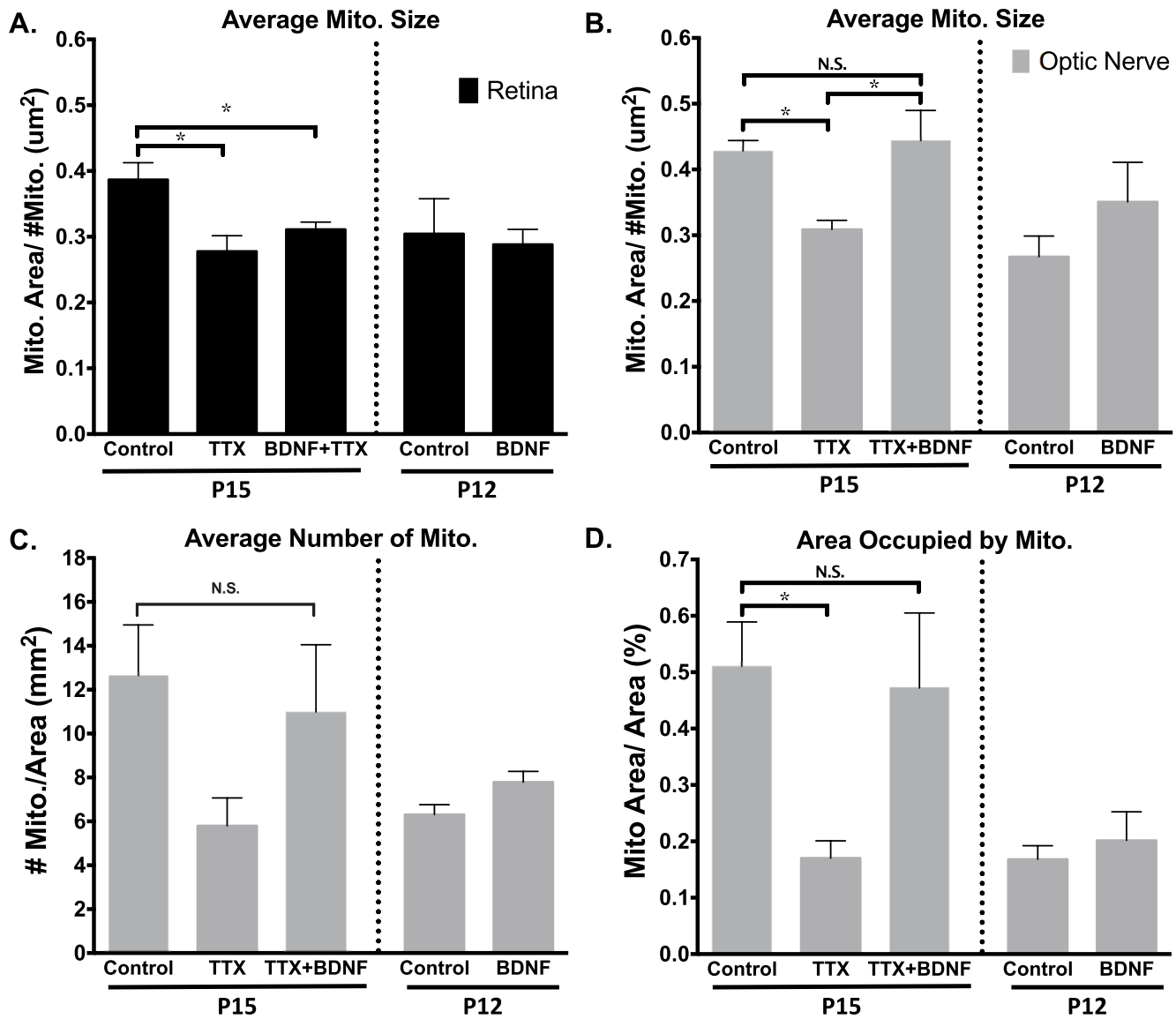
**Figure 1.** Axonal mitochondria increase in size, number and area through eye development. CFP+ mitochondria were imaged by confocal microscopy and analyzed in ImageJ. (A) Example image of mitochondrial labeling within retinal RGC axon segments (50um scale bar) and (B) in optic nerve RGC axon segments from postnatal day 9 (P9), P12, P15, and P45 mice (1um scale bar). (C-E) In both retinal and optic nerve RGC axons, the average mitochondrial size, number, and area (measured as percent of cross sections, representing fractional volume) increased from P9 to adulthood. (Error bars indicate SEM;  $N \geq 3$  mice per age, with 9 images analyzed per animal; one-way ANOVA with Holm-Sidak correction for multiple comparisons, \*  $p \leq 0.05$ .)



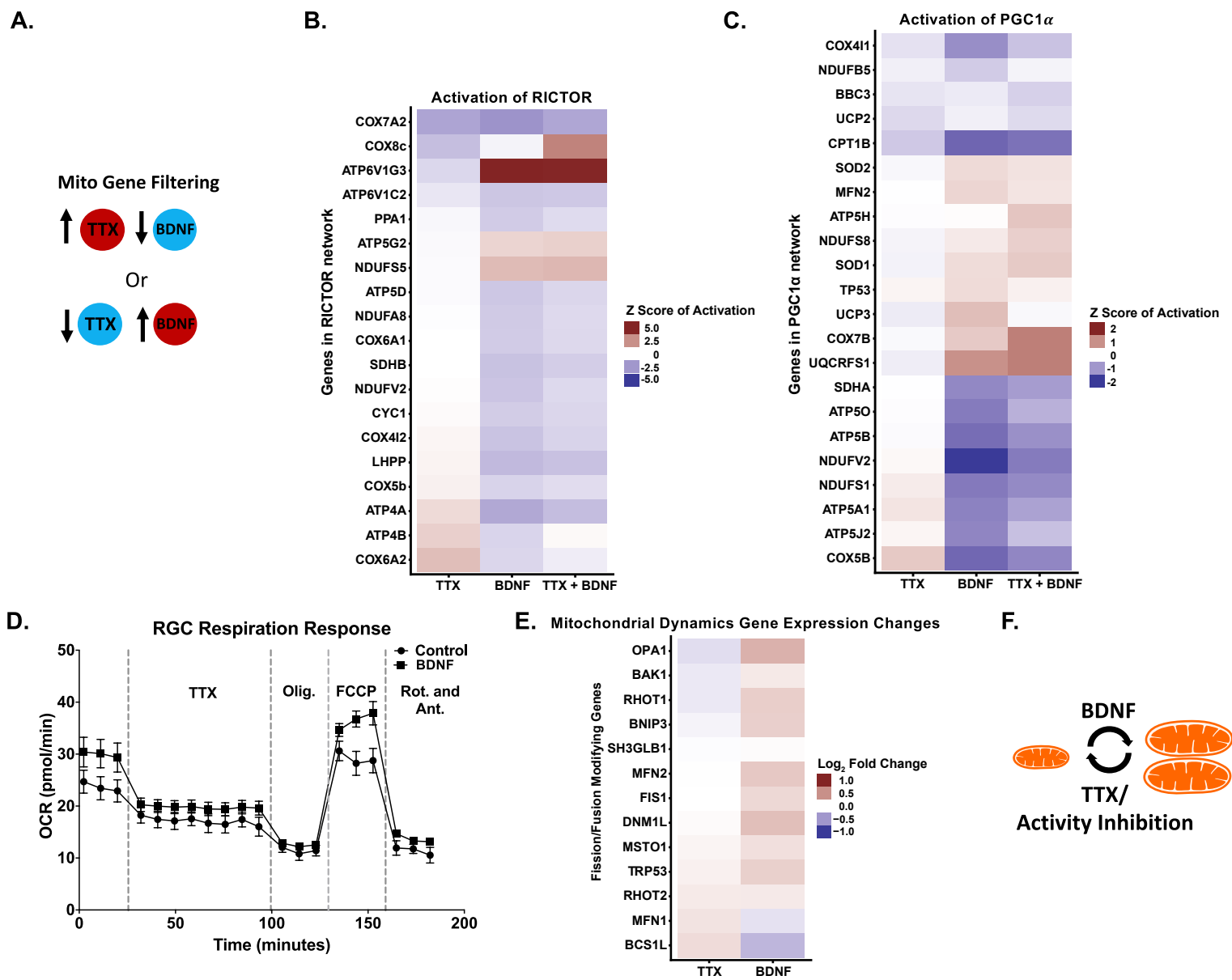
**Figure 2.** Mitochondrial size and number increase at eye opening in RGC axons. (A) Mitochondria were imaged and quantified in RGC optic nerve axons by transmission electron microscopy before (P12) and after (P15) eye opening. Increased magnification (insets) shows mitochondrial membrane, cristae, and representative mitochondrial size differences. Scale bar 500 nm. (B) Average mitochondrial size, (C) number and (D) area increased significantly between P12 and P15. (Error bars indicate SEM;  $n \geq 30$  sections; t-test \*  $p < 0.05$ ).



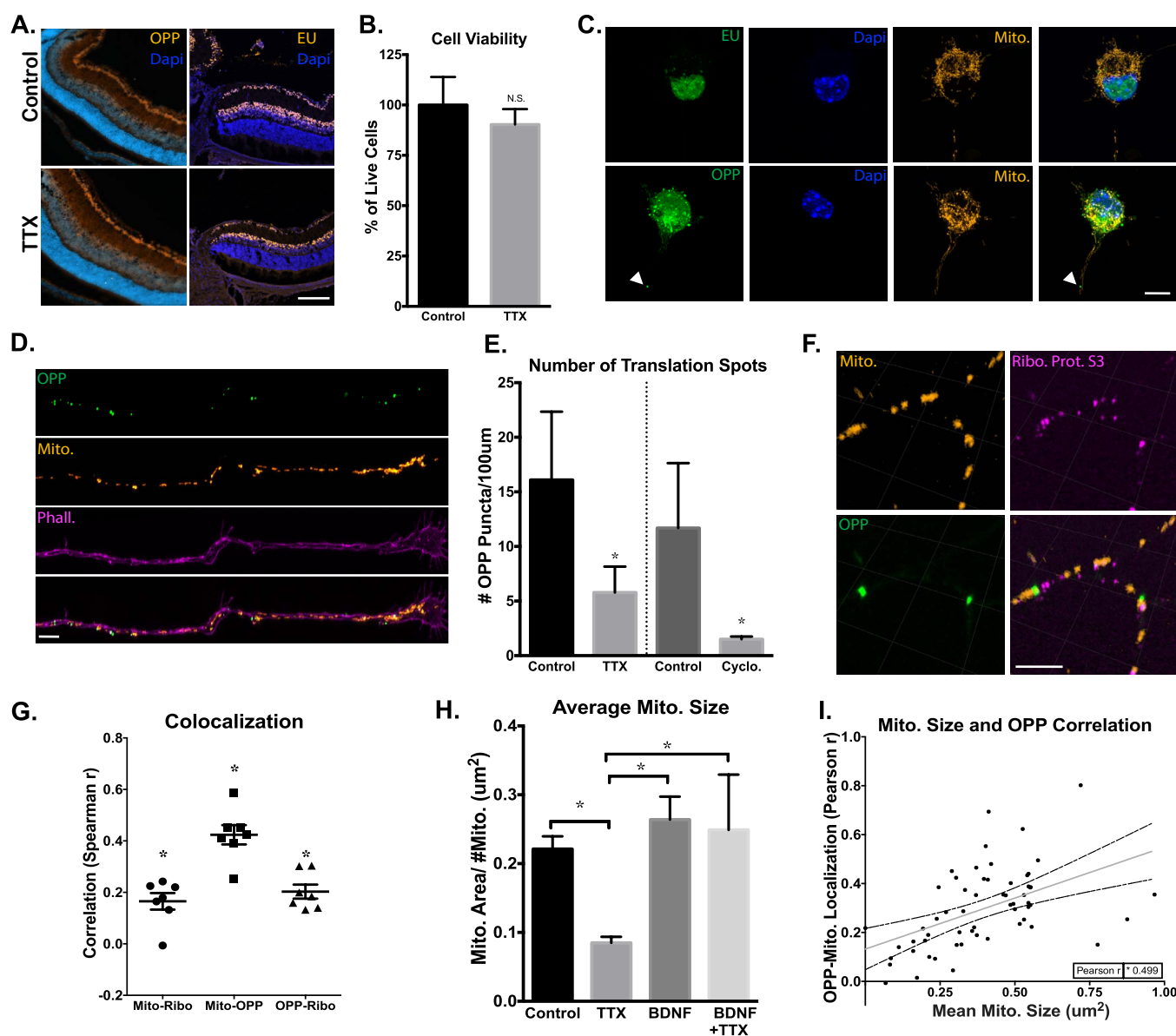
**Figure 3.** Eye opening is sufficient and necessary developmental changes in mitochondrial size and localization. (A) Surgical model for premature eye opening and sutured eyelid closure. (B) Average mitochondrial size, (C) number, and (D) area increase with premature eye opening, and this developmental increase is inhibited by prolonged eye closure. (Error bars indicate SEM;  $N \geq 3$  mice per condition, 9 images analyzed per animal; Students t-test \*  $p < 0.05$ .)



**Figure 4.** Mitochondrial developmental changes are dependent on retinal electrical activity and are partially rescued by BDNF in optic nerve axons. Control, TTX- or TTX plus BDNF-treated mice analyzed at P15, as well as control or BDNF-treated mice analyzed at P12 are graphed on the same axis for comparison, but the experiments were performed and analyzed separately. Measured changes in (A) average mitochondrial size within retinal axons and (B) optic nerve axons, as well as the corresponding mitochondrial (C) number and (D) area. (Error bars indicate SEM; N= 3 mice per condition, 9 images analyzed per animal; one-way ANOVA with Newman-Keuls multiple comparisons test (A-C) or Fisher LSD test (D), \* p < 0.05)

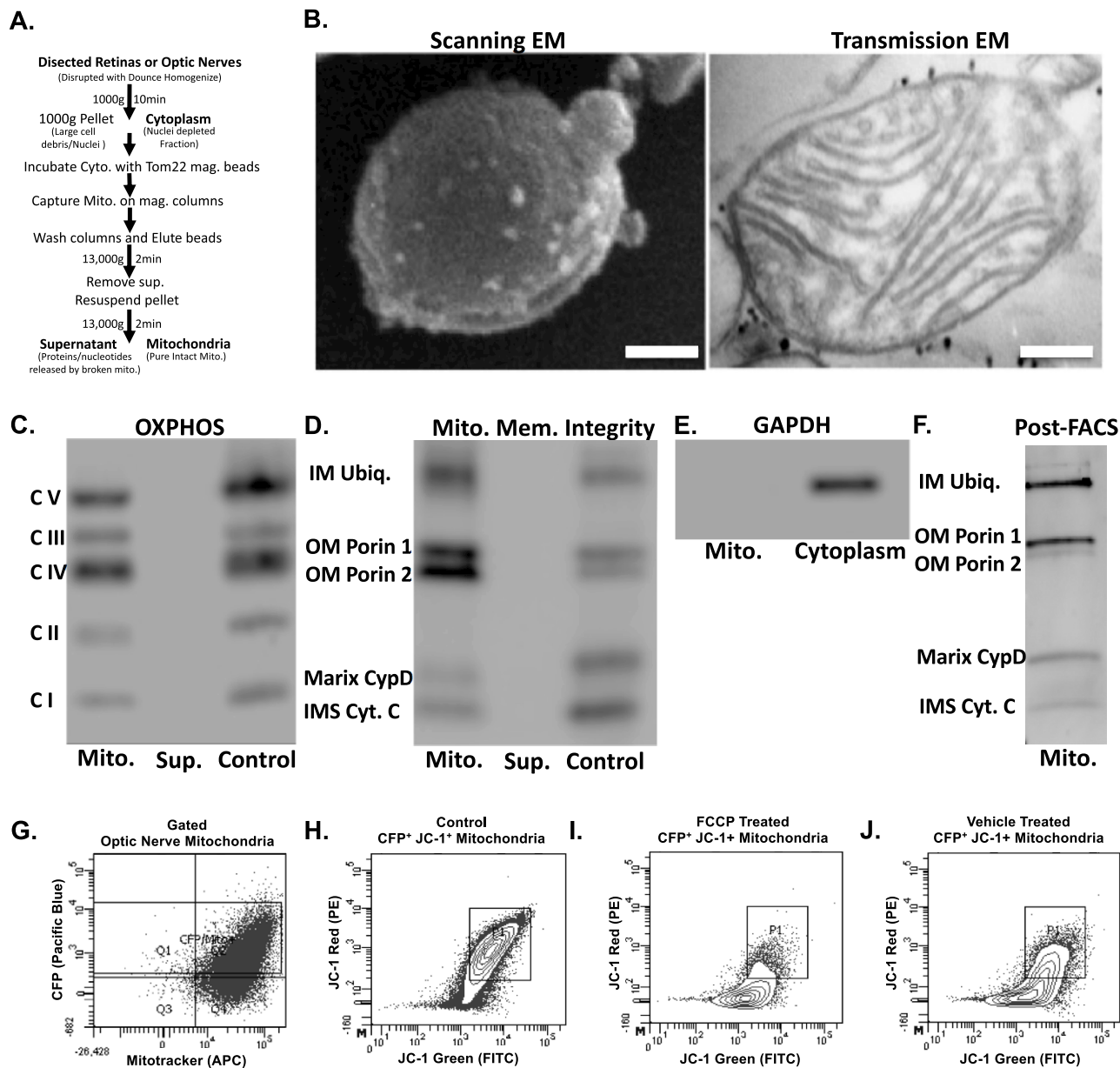


**Figure 5.** RGC nuclear-encoded mitochondrial gene expression in response to activity inhibition with TTX and/or BDNF is consistent with inhibition versus activation of mitochondrial dynamics and energetics. (A) Model for filtering data acquired from RT-PCR gene array analysis of P15 acutely purified RGCs, after TTX and/or BDNF intravitreal injections at P11 and P13 (N=3 RGC preps per condition). Filters were placed to identify gene expression regulated in opposing directions by BDNF and TTX. The resulting genes were then passed through IPA® pathway analysis software, which suggested 10 major upstream regulators, with PGC1- $\alpha$  and RICTOR at the top of the list. Downstream gene expression data modulated by these upstream regulators were transformed into Z-score of activation. Up- or downregulated gene sets are denoted by color. (B) Genes identified in our array that are regulated by RICTOR represent mainly energetics genes. (C) Genes identified in our array that are regulated by PGC1- $\alpha$  represent mainly mitochondrial dynamics and biogenesis regulators. (D) Measuring the effect of BDNF on mitochondrial dependent oxygen consumption in purified RGCs shows an increase in the basal respiration rate, and maximum respiration capacity (with FCCP addition) regardless of activity inhibition by TTX (introduced 35min after initial recording). TTX, Oligomycin, FCCP, and Rotenone/Antimycin A, were added sequentially at time points marked with vertical lines. Recorded values were acquired using the Seahorse XF96 instrument (Error bars indicate SEM; n=6 replicates per condition, pooled from 3 separate RGC preps and assayed on one plate) (E) Genes identified in our array that have been previously demonstrated as mitochondrial fission/fusion or mitochondrial size modifying are oppositely regulated by TTX and BDNF, with most genes upregulated by BDNF. (F) Model of the predicted mitochondrial events triggered by TTX or BDNF, based on gene pathway analysis and the identified mitochondrial changes in injected mice.

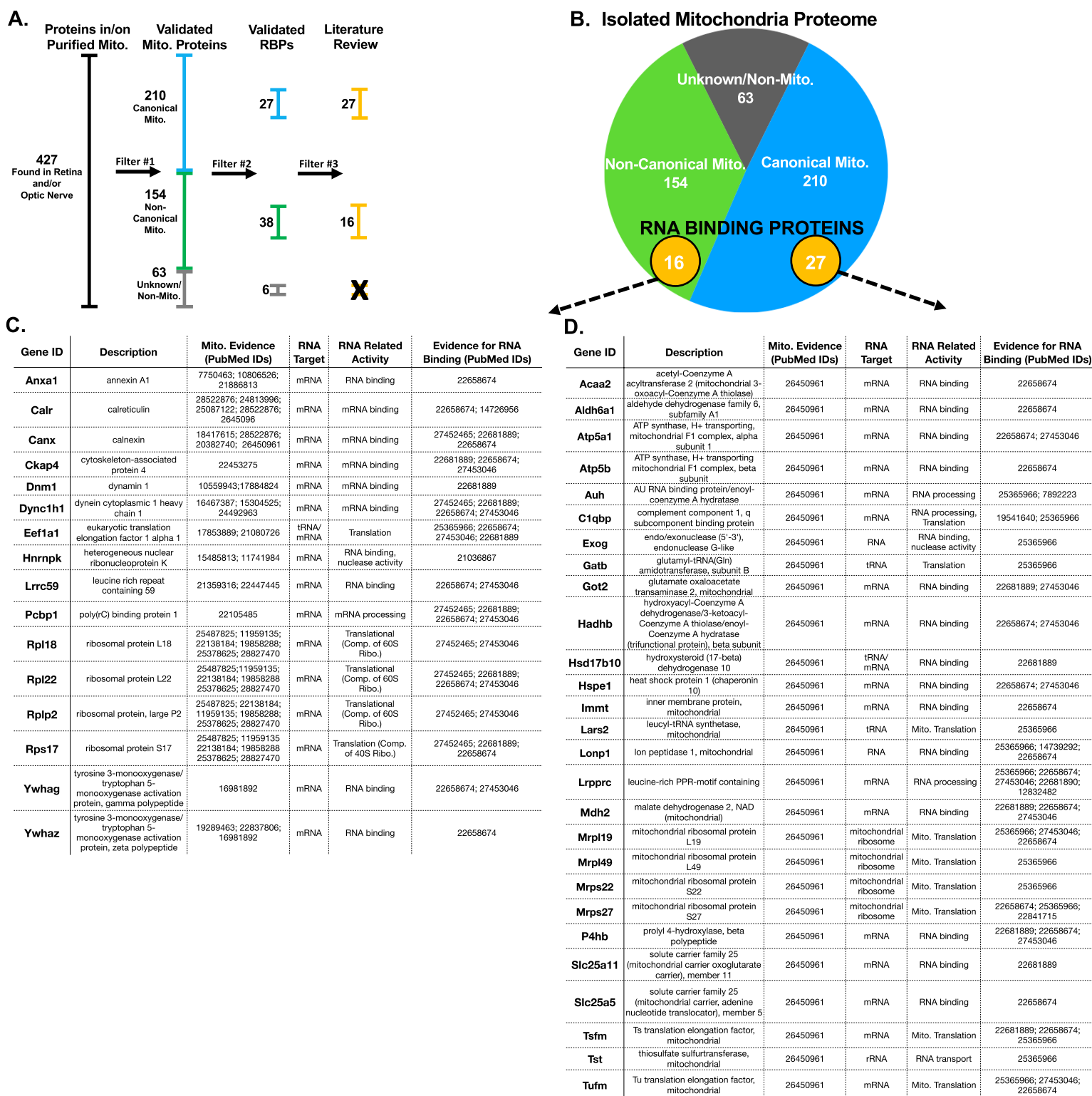


**Figure 6.** Activity regulates mitochondrial localized protein translation in axons. (A) Representative images collected by confocal microscope of P15 retinas, after in vivo intravitreal injections of TTX or BSS (control) at P11 and P13, and an injection of EU or OPP 2 hours before dissection and tissue processing. There were no detectable differences in EU or OPP fluorescence in the retina after TTX-mediated inhibition of activity (100μm scale bar). (B) Cell viability of TTX- and-control treated RGCs, identified as Calcein-AM positive and Sytox negative, normalized for total cell number by Hoescht, and quantified as percent change relative to control treated cells (Error bars indicate SEM; N=3 replicate RGC preps, n>100 cells per replicate condition; Student's t-test, \*p < 0.05). (C) Confocal images of cultured RGCs treated with BacMam virus, labeling mitochondria with DsRed, and pulsed with EU for 1hr or OPP for 15 min before fixation and staining for newly synthesized RNA and protein, respectively. EU RNA and OPP protein staining were strongly detected in RGC nuclei and cell bodies, and newly translated proteins were also detected in axons (marked by arrows, 10μm scale bar). (D) Axon tips demonstrate strong OPP+ puncta throughout growth cone and terminal axon domains. OPP-labeled with Alexa488, mitochondria with DsRed, and axon tips with phalloidin Alexa647 (5μm scale bar). (E) Quantified average number of OPP puncta per 100 μm of P4 RGC's axon termini, treated with TTX or cycloheximide and with vehicle treated controls. Groups separated by vertical line were experimentally treated and analyzed separately (Error bars indicate SEM; n>10 randomly imaged axons, selected from 3 replicate RGC preps; Student's t-test, \*p < 0.05). (F) Representative image of mitochondria, OPP-labeled new protein synthesis, and ribosomal protein S3 colocalization within axons (1μm scale bar), along with (G) the spearman correlation values for the association of OPP to Mito, Mito to Ribosomes, and Ribosomes to OPP signals in line-scanned axons (Error bars indicate SEM; n=7 randomly imaged axons, selected from 3 replicate RGC preps; individual R values were all significant, \*p < 0.05). (H) Quantified mean mitochondrial size in axons from RGCs incubated with TTX, BDNF, TTX and BDNF, or vehicle controls (Error bars indicate SEM; n>10 randomly imaged axons, from 3 replicate RGC preps; one-way ANOVA with Holm-Sidak's test, \*p < 0.05). (I) Pearson's correlation values from a pixel by pixel analysis for OPP-mitochondrial colocalization relative to mean mitochondrial size, demonstrating a significant and positive correlation between increasing OPP colocalization and mitochondrial size (Regression line and 95% confidence intervals are plotted, data points from n>30 randomly imaged axons, selected from 3 replicate RGC preps; Pearson r was significant, \*p < 0.05).

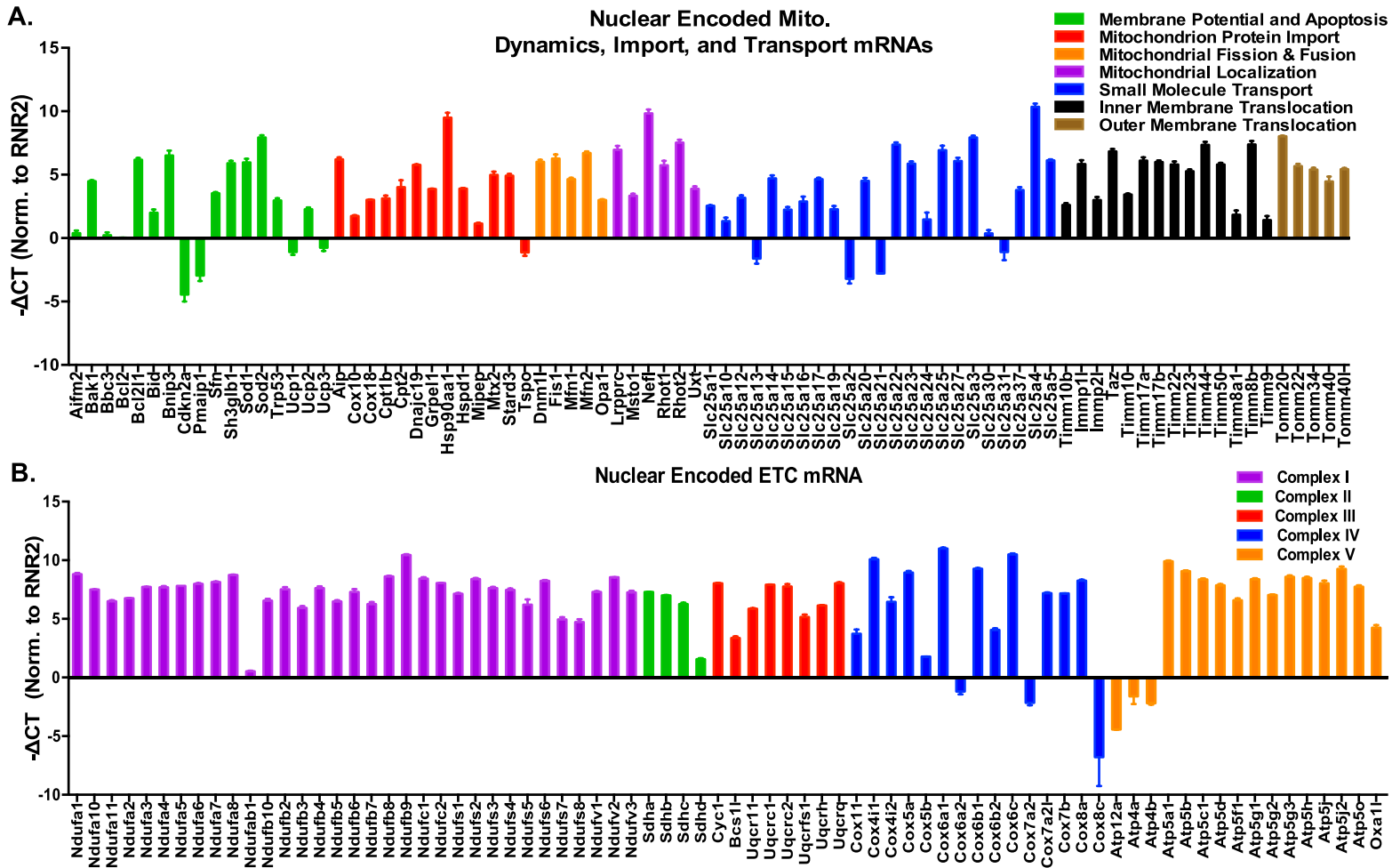




**Figure 7.** Purified mitochondria retain their protein content and membrane integrity. (A) Outline of mitochondrial isolation and subsequent assays. (B) TOM22-bound nanoparticles are visible, bound to the outer mitochondrial membrane in both SEM (white spots) and TEM (black dots). Scale bars 50 nm and 100 nm. (C-F) Western blot analyses of purified mitochondria and supernatants. Magnetically isolated mitochondria retain (C) OXPHOS subunits, as well as (D) outer membrane (OM), inner membrane (IM), and inner membrane space (IMS) proteins. (E) GAPDH is detectable in cytoplasmic but not mitochondrial isolate fractions. (F) FACS-sorted mitochondria retain both inner and outer membrane integrity proteins. (G) FACS-isolated mitochondria are intact and viable, retaining CFP and fluorescing with membrane potential-dependent mitotracker CMXROS. (H) Sorted CFP+ mitochondria demonstrate polarization-dependent fluorescence with JC-1, and (I) lose membrane potential with FCCP depolarization to a greater degree than (J) vehicle-treated controls.



**Figure 8.** Proteomics mass spectrometry analysis reveals nuclear-encoded RNA binding proteins associated with purified mitochondria. (A) Filtering used to identify mitochondria-specific proteins and proteins with RNA binding properties. (B) Venn diagram of total protein hits sorted by annotation in the MitoCarta database. (C,D) Candidate mitochondria-associated RNA binding proteins with cited evidence (PubMed ID shown) for their functional RNA binding role and mitochondrial interaction (N=6 mitochondrial purifications).



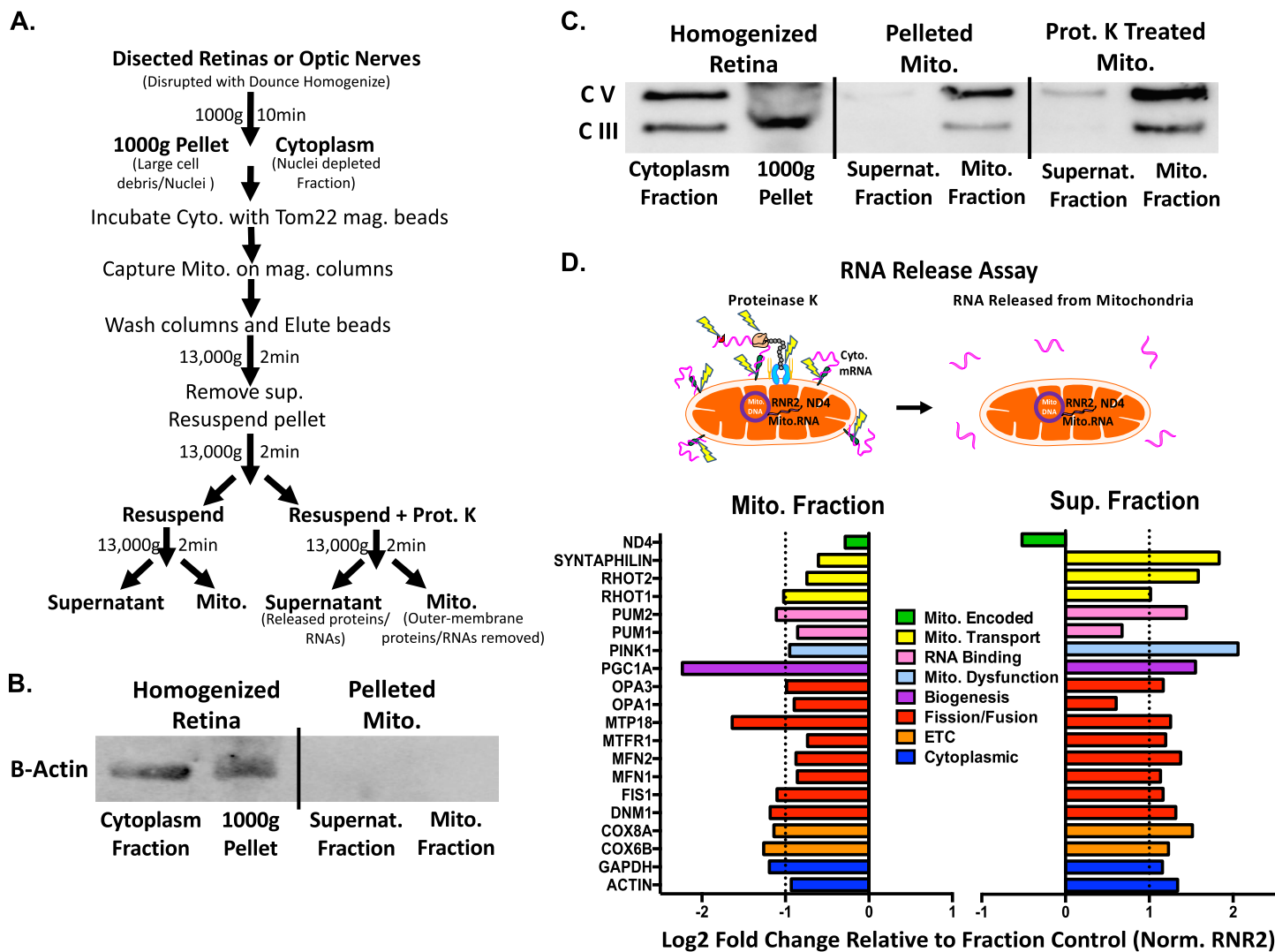


**Figure 10.** Purified mitochondria bind nuclear-encoded mRNAs through outer membrane-associated proteins. (A) Outline of mitochondrial isolation and subsequent assays. (B)  $\beta$ -actin is detected in homogenized retina but not in purified mitochondria. (C) Mitochondrial pellets treated with proteinase K retain inner matrix proteins, Complex III-Core Protein 2 (UQCRC2) and Complex V alpha subunit (ATP5A), confirming that proteinase K only strips off outer membrane-associated proteins. (D) Proteinase K-treated mitochondria release bound RNA into the supernatant fraction, as detected by qPCR of pelleted mitochondrial fraction and corresponding supernatant fractions. Data normalized to control mitochondrial fraction and RNR2, graphed as a log<sub>2</sub> fold change to represent up and down regulation of RNA. Dotted line represents changes greater than 2-fold ( $n=3$  replicates from a mito. purification).

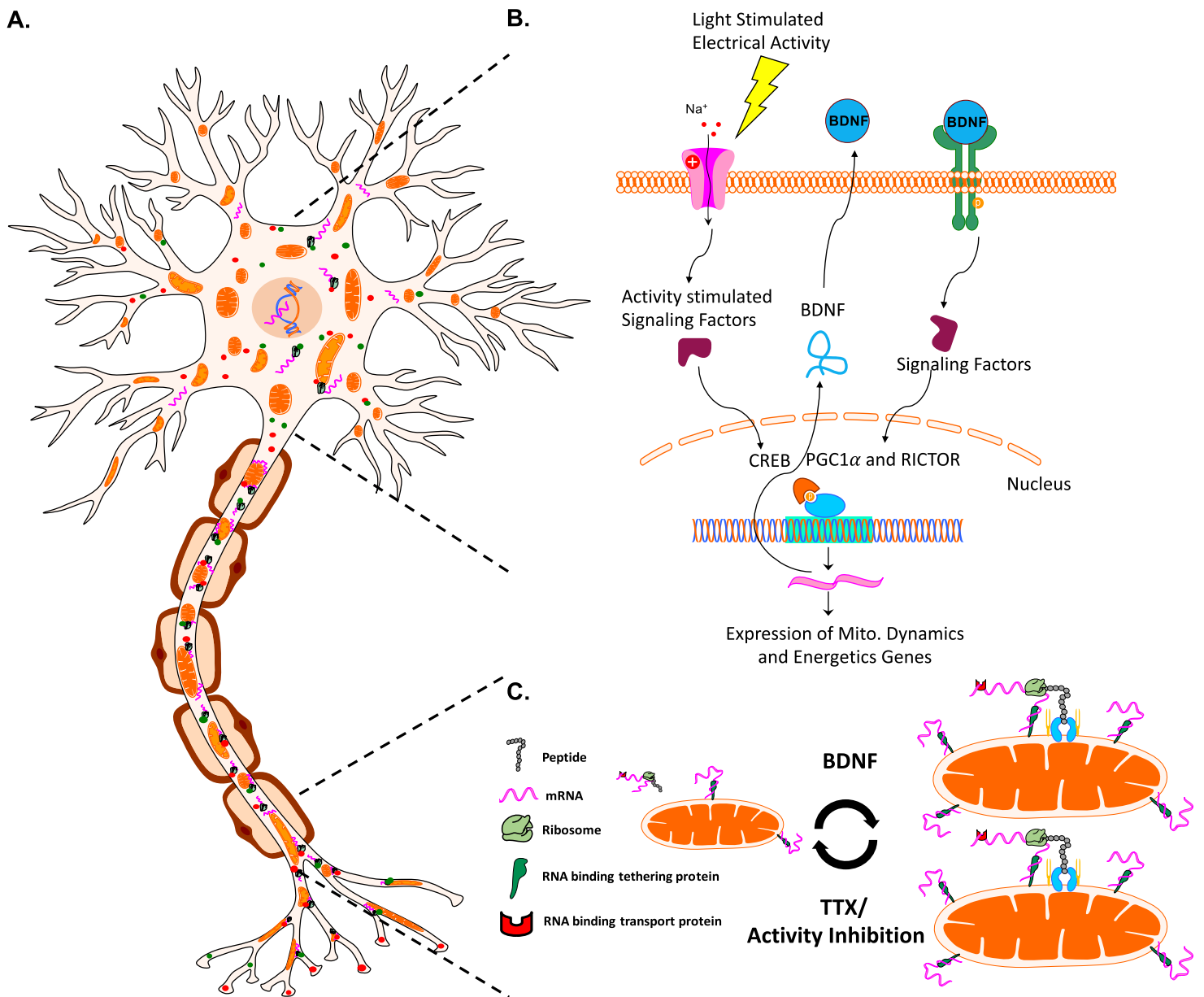


**Figure 11.** A model for activity- and BDNF-regulated mitochondrial size, number, and associated protein translation. (A) Neurons contain mitochondria, RNA, RNA binding and transport proteins, ribosomes, and newly synthesized proteins, throughout distal axon and dendrite compartments. (B) Electrical activity in RGCs, for example driven by light stimulation of retinal circuitry after eye opening, activates a signaling pathway that culminates in the activation of transcription factors such as CREB, and the expression of BDNF. BDNF signaling stimulates nuclear-encoded mitochondrial gene expression, coordinated by the activation of transcriptional regulators RICTOR and PGC1- $\alpha$ . (C) Neuronal activity and downstream BDNF signaling stimulates increases in mitochondrial size and number, reversed by activity inhibition. Changes in mitochondrial size also correlate with mitochondrial localized translation of nuclear-encoded transcripts.